Theoretical and numerical study of a symmetrical triple flame using the parabolic flame path approximation

By SANDIP GHOSAL† AND LUC VERVISCH

LMFN, INSA-Rouen, UMR – CNRS 6614/CORIA,
Saint-Etienne-du-Rouvray, 76801 Cedex, France

In non-premixed turbulent combustion the reactive zone is localized at the stoichiometric surfaces of the mixture and may be locally approximated by a diffusion flame. Experiments and numerical simulations reveal a characteristic structure at the edge of such a two-dimensional diffusion flame. This 'triple flame' or 'edge flame' consists of a curved flame front followed by a trailing edge that constitutes the body of the diffusion flame. Triple flames are also observed at the edge of a lifted laminar diffusion flame near the exit of burners. The speed of propagation of the triple flame determines such important properties as the rate of increase of the flame surface in non-premixed combustion and the lift-off distance in lifted flames at burners. This paper presents an approximate theory of triple flames based on an approximation of the flame shape by a parabolic profile, for large activation energy and low but finite heat release. The parabolic flame path approximation is a heuristic approximation motivated by physical considerations and is independent of the large activation energy and low heat release assumptions which are incorporated through asymptotic expansions. Therefore, what is presented here is not a truly asymptotic theory of triple flames, but an asymptotic solution of a model problem in which the flame shape is assumed parabolic. Only the symmetrical flame is considered and Lewis numbers are taken to be unity. The principal results are analytical formulas for the speed and curvature of triple flames as a function of the upstream mixture fraction gradient in the limit of infinitesimal heat release as well as small but finite heat release. For given chemistry, the solution provides a complete description of the triple flame in terms of the upstream mixture fraction gradient. The theory is validated by comparison with numerical simulation of the primitive equations.

1. Introduction

In many engineering applications of turbulent combustion, fuel and oxidizer are not perfectly mixed before entering the combustion chamber. Large-scale unsteady movements together with micro-mixing mechanisms subsequently bring fuel and oxidizer into contact where they react within a thin reaction zone (Bray 1996) that may be locally approximated by a diffusion flame. A typical example is given in figure 1 which shows an instantaneous reaction rate profile from a two-dimensional

† Present address: Northwestern University, Department of Mechanical Engineering, 2145 Sheridan Road, Evanston, IL 60208, USA.
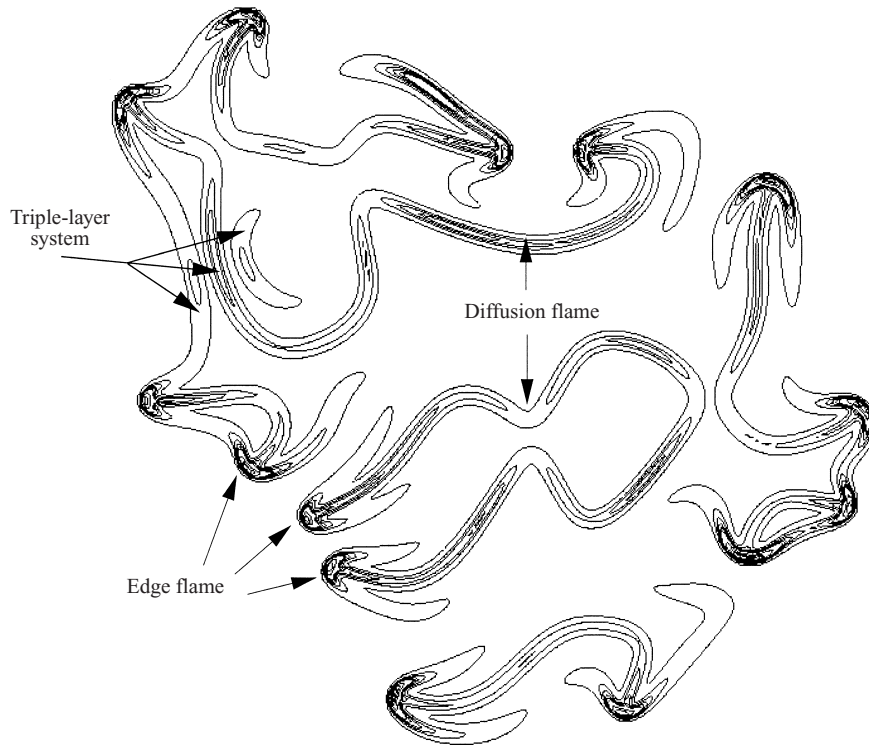
FIGURE 1. Isolines of reaction rate in a two-dimensional simulation of combustion in pockets of fuel and hot air in freely decaying turbulence (Vervisch & Poinsot 1998).

simulation of the propagation of combustion in pockets of fuel and hot air in freely decaying turbulence (Vervisch & Poinsot 1998).

A generic picture of such a laminar diffusion flame was given by Liñán & Crespo (1976) for a counterflowing fuel and oxidizer stream with a single-step chemical reaction. The flame is localized at the stoichiometric surface where fuel and oxidizer are mixed in stoichiometric proportions, and their analysis provides a full description of the flame in terms of the local mixture fraction gradient normal to the flame front. In this quasi-steady diffusion flame, the gradients of chemical species and temperature are such that the amount of heat diffusing away from the reaction zone is exactly balanced by the heat produced by combustion. Should the local gradient of temperature become too large, the rate of chemical reactions is not able to keep up with the heat losses and quenching occurs.

Applying this description to the above picture of non-premixed turbulent combustion, one expects that the reaction zone would be confined to the highly convoluted stoichiometric surface; however, the reaction rate would not be uniform over the surface. Instead, there would be zones where excessive thermal gradients cause local extinction of the flame. This is shown schematically in figure 2. Such enhanced thermal gradients are expected to occur in a turbulent fluid where velocity fluctuations would cause the flame to stretch. When these thermal gradients are subsequently reduced below the quenching limit through turbulent fluctuations, the diffusion flame may propagate along the stoichiometric surface, re-igniting the quenched zones. The characteristic flame structure that is observed at the edges of the stoichiometric sur-
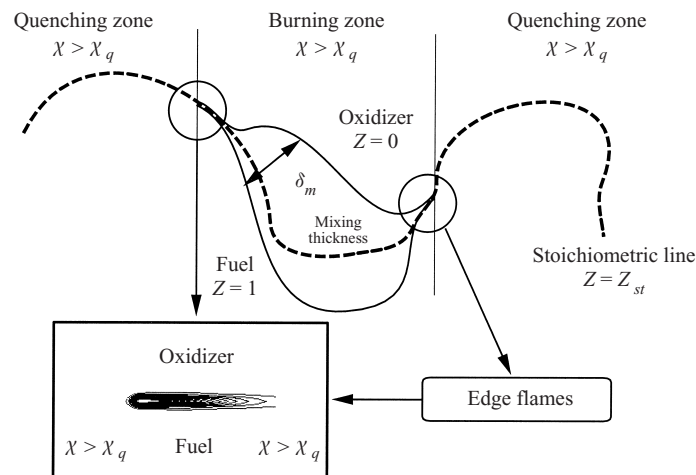
FIGURE 2. Sketch of the conditions for the development of partially premixed edge flames in non-premixed turbulent flames. $\chi = D|\nabla Z|$ is the mixture fraction dissipation rate and χ_q the quenching limit (Vervisch & Poinsot 1998).

face bordering the extinction zone can be modelled locally by a triple flame. Such structures are clearly visible in figure 1.

The simplest laboratory situation where a triple flame may be observed is at a lifted flame downstream of a splitter plate separating fuel and oxidizer. The leading edge of this lifted flame is a partially premixed front that tends to propagate towards the fresh gases upstream but is stabilized by the counterflowing stream blowing off the splitter plate. Since premixed flame speeds are maximum for stoichiometric or near stoichiometric conditions, the parts of the flame front on the stoichiometric line tend to move faster than those further out, causing the flame front to be curved with the convex side facing the splitter plate. Behind this partially premixed front, two streams, one depleted of fuel and the other of oxidizer, come together and burn as a diffusion flame. This trinity consisting of a partially premixed fuel-rich branch, a partially premixed fuel-lean branch and a diffusion flame anchored behind it is called a 'triple flame'. Figure 3 shows an expanded view of a single triple flame as revealed by numerical simulation of the basic equations. The isocontours denote constant reaction rates.

Experimental, theoretical and numerical studies have been performed to explore both the conditions leading to the existence of triple flames and their properties. The first reported observation of the triple flame in the laboratory is due to Phillips (1965). Kioni *et al.* (1993) have studied the development of a partially premixed front in a mixing layer without velocity shear using a burner designed to create a linear profile of fuel mixture fraction in a mixture of fuel and air. Measurements and calculations of species distributions within the edge of a lifted laminar axisymmetric diffusion flame have been presented by Plessing *et al.* (1998). Choi, Ko & Chung (1998) have also observed triple flames in experimental investigations of the characteristics of flame propagation around a non-premixed vortex ring. From direct numerical simulations (DNS) of the autoignition of non-premixed turbulent mixtures, Domingo & Vervisch (1996) have concluded that triple flames play an important role in the spreading of the reactive zones. Also using DNS, Favier & Vervisch (1998) have investigated the effects of edge flames and triple flames in turbulent flame lift-off. Numerics was also utilized
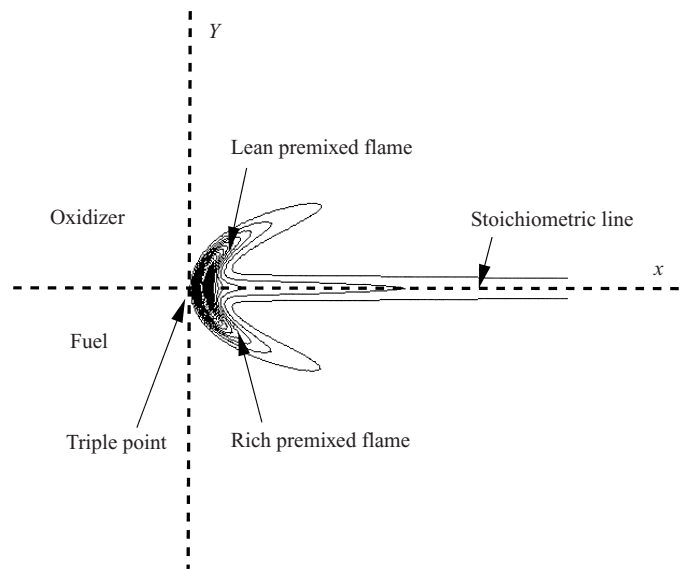
FIGURE 3. The structure of an isolated propagating triple flame as observed in direct numerical simulation. The contours are isolines of heat release or reaction rate (Ruetsch *et al.* 1995).

by Ruetsch, Vervisch & Liñán (1995) to address the relation between heat release and triple-flame velocities, and by Echekki & Chen (1998) to study the chemical structure of methanol–air triple flames. Theoretical investigations were undertaken by Buckmaster & Matalon (1988) to study Lewis number effects, theoretical results on propagation velocity and shape of triple flames were derived by Dold (1989) and Hartley & Dold (1991) and edge-flame holding was studied by Buckmaster & Weber (1996).

The first theoretical derivation of the speed of propagation of a triple flame is due to Dold (1989). In this analysis Dold assumed the fuel mixture fraction gradient to be weak so that the triple flame would have only a slight curvature. This restriction was later removed by Hartley & Dold (1991). However, in both analyses, density perturbations due to heat released in the combustion were neglected to keep the problem tractable. Nevertheless, the importance of such variable-density effects have been pointed out by Ruetsch *et al.* (1995) through analysis of results of numerical simulation. The present work is an attempt to include at least the lowest-order effect of such density changes. In the present work, we assume unity Lewis numbers. The effect of small deviations from unity Lewis numbers have recently been studied by Daou & Liñán (1998) in the incompressible limit for weakly curved flames.

We first revisit the constant-density case, but using an approach that is different from that of Hartley & Dold. The essential difference is that, instead of treating the flame surface as an unknown free boundary, we approximate it by a parabolic profile (albeit of unknown curvature). While this is reasonable in the immediate vicinity of the flame tip, it has no formal justification for distances from the flame tip of the order of or greater than the radius of curvature of the flame front. However, since the reaction rate drops steeply with distance from the flame tip (see figure 4), it is hoped that the inaccurate representation of the flame path away from the tip would have a negligible impact on quantities of physical interest such as propagation speed. We call this the 'parabolic flame path approximation'. We then apply the method of
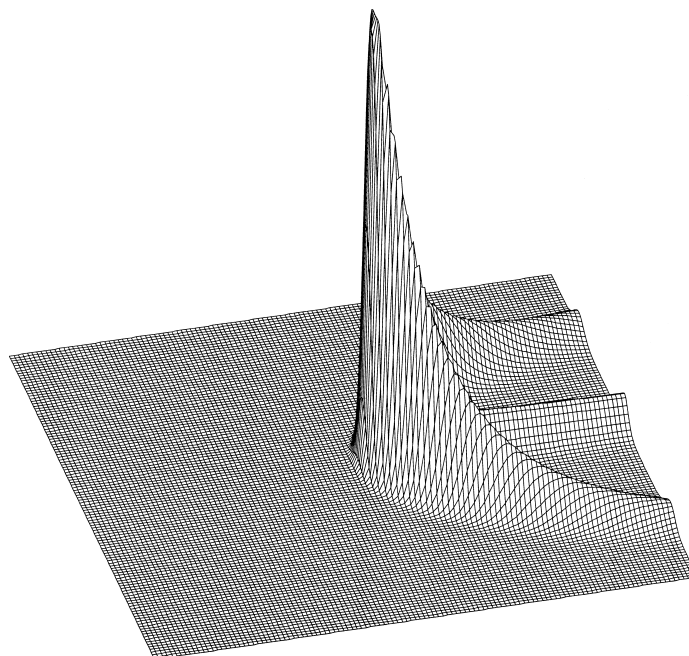
FIGURE 4. The reaction rate of a triple flame (vertical axis) as a function of X and Y as observed in direct numerical simulations (Ruetsch *et al.* 1995).

matched asymptotic expansions in parabolic-cylinder coordinates, thereby obtaining closed form expressions for the flame curvature and velocity as well as the temperature field. Comparisons between these theoretical results and numerical simulations of the primitive equations are also presented.

The case of small, but finite, heat release is then investigated by treating the density change as a linear perturbation of the earlier constant-density solution. The deviation of the flow due to variable-density effects can then be obtained in closed form. This enables us to calculate the effects of streamline curvature on the flame speed. The results are consistent with those obtained from numerical simulation of the fully compressible primitive equations and the qualitative arguments first proposed by Ruetsch *et al.* (1995). For a given chemistry, the approximate solution provides a complete description of the triple flame in terms of a single parameter, the upstream mixture fraction gradient.

The paper is organized as follows. In the next section the problem is formulated and the basic equations are given. Appropriate dimensionless parameters are introduced and the physically relevant region of parameter space is identified. We then introduce the approximation of low heat release and present a simplified set of equations describing this situation. The method for introducing the lowest-order correction for heat release effects is also outlined here. In §3 we solve the low-heat-release (constant-density) problem in the limit of large Zeldovich number. Comparisons with numerical simulation as well as the earlier asymptotic results of Hartley & Dold are presented here. In §4 the effect of a density perturbation due to heat release is treated in the limit of linear theory. Comparisons are presented with numerical simulations of the primitive equations describing compressible reacting flows. The main results of the paper are summarized in §5.

2. Problem formulation

We consider a simple one-step combustion process where v_0 molecules of a fuel (molecular mass m_0) react with v_1 molecules of an oxidizer (molecular mass m_1) to form v_p product molecules (molecular mass m_p). The reactants and products are assumed to be in the gaseous phase. Most combustion processes in nature and in industry are multi-step processes involving a fairly large number of intermediate species. The restriction to a single-step process is made in order to have a tractable problem. Finally, we will only consider the case of unity Lewis number (that is, temperature and each of the two species diffuse at the same rate). This enables one to express the species concentrations as a linear combination of just two variables: the temperature, which evolves according to an advection-reaction-diffusion equation, and the mixture fraction, which evolves like a passive (non-reactive) scalar.

2.1. *Basic equations*

The time evolution of the mass fractions of the two reacting species, Y_0 (the fuel) and Y_1 (the oxidizer), is described by

$$\rho \frac{\mathrm{D}Y_i}{\mathrm{D}t} = D_i \nabla^2 Y_i - v_i m_i \omega, \tag{2.1}$$

where $i = 0$ or 1, $\mathrm{D}/\mathrm{D}t = \partial/\partial t + \boldsymbol{u} \cdot \nabla$ is the material derivative, ρ and $\boldsymbol{u}$ are the fluid density and velocity, ω is the number of reactions in unit volume per unit time and D_i is the mass diffusivity of species i. The evolution of the temperature, T, is described by

$$\rho c_p \frac{\mathrm{D}T}{\mathrm{D}t} - \frac{\mathrm{D}p}{\mathrm{D}t} = D_T \nabla^2 T + Q\omega, \tag{2.2}$$

where p is the pressure, c_p the specific heat at constant pressure referred to unit mass of gas, Q is the amount of heat released per reaction and D_T is the thermal conductivity. The Lewis numbers will be assumed unity in this work so that

$$\frac{D_0}{\rho_\infty} = \frac{D_1}{\rho_\infty} = \frac{D_T}{\rho_\infty c_p} \equiv k, \tag{2.3}$$

where ρ_∞ is the density of unburnt gas far upstream (assumed constant). The effect on the flame propagation speed of non-unity Lewis numbers has recently been presented for weakly curved flames (without heat release) and Lewis numbers close to unity by Daou & Liñán (1998). The equation of state is that of an ideal gas,

$$p = \frac{\rho k_B T}{m}, \tag{2.4}$$

where k_B is Boltzmann's constant and m is the mean molecular weight. For the reaction rate, ω, we assume the well known Arrhenius law (Liñán & Williams 1993):

$$\omega = A\rho^{v_0+v_1} Y_0^{v_0} Y_1^{v_1} \exp(-T_a/T), \tag{2.5}$$

where T_a is the activation temperature (a constant for a given reaction) and the pre-exponential factor A can in general have a weak temperature dependence. However, we will take A to be constant for simplicity. The density changes are coupled to the velocity field through the equation of mass conservation

$$\frac{\partial \rho}{\partial t} + \nabla \cdot (\rho \boldsymbol{u}) = 0. \tag{2.6}$$

It follows from the momentum equation that the pressure fluctuation $(p-p_\infty)/p_\infty \sim$

M^2, where p_∞ is the upstream pressure and M is a Mach number defined as the ratio of flame to sound propagation speeds. Typically $M \ll 1$ in the problems we are interested in (for example, the burning speed of a stoichiometric mixture of pure methane and air under standard laboratory conditions is $\approx 0.4\,\mathrm{m\,s^{-1}}$ corresponding to $M \approx 10^{-3}$). Therefore, to a very good approximation, the density can be expressed as a function of temperature,

$$\rho = \frac{mp_\infty}{k_B T}, \tag{2.7}$$

and, the Dp/Dt term in (2.2) may be dropped, so that the temperature equation becomes

$$\rho c_p \frac{DT}{Dt} = k\rho_\infty c_p \nabla^2 T + Q\omega. \tag{2.8}$$

We will consider the problem from a frame of reference in which the triple flame is stationary (see figure 3). The origin of the coordinate system is fixed at the tip (triple point) of the curved flame front and a uniform flow, $U_\infty \hat{x}$, is incident from $x = -\infty$. Clearly, U_∞ is also the propagation speed of the triple flame in a frame in which the fluid far from the flame is stationary. Far upstream ($x \to -\infty$) we assume that the fuel mass fraction varies from $Y_0 = 1$ in the fuel stream ($y \to +\infty$) to $Y_0 = 0$ in the oxidizer stream ($y \to -\infty$). Similarly, the oxidizer mass fraction varies from $Y_1 = 1$ ($y \to -\infty$) to $Y_1 = 0$ ($y \to +\infty$), such that

$$Y_0(-\infty, y) + Y_1(-\infty, y) = 1 \tag{2.9}$$

if the reactants are not diluted with an inert species. The fuel and oxidizer are assumed to be at the same constant temperature, $T = T_\infty$, far upstream and the density far upstream is also a constant, $\rho = \rho_\infty$. The fuel mixture fraction, Z, is then

$$Z = \frac{rY_0 - Y_1 + 1}{1 + r}, \tag{2.10}$$

where $r = (v_1 m_1)/(v_0 m_0)$. Clearly, $Z = 1$ in the fuel stream, $Z = 0$ in the oxidizer stream and $Z = Z_s = 1/(1 + r)$ under stoichiometric conditions.

It follows from (2.1) and (2.10) that Z evolves as a passive scalar:

$$\rho \frac{DZ}{Dt} = k\rho_\infty \nabla^2 Z. \tag{2.11}$$

By eliminating the source terms from the pair of equations (2.8) and (2.1), it may be shown that, the 'Shvab–Zeldovich variables' (Liñán & Williams 1993) $H_i = T + QY_i/(v_i m_i c_p)$ also evolve as a passive scalar:

$$\rho \frac{DH_i}{Dt} = k\rho_\infty \nabla^2 H_i. \tag{2.12}$$

From (2.10) and (2.9) and the condition that $T = T_\infty$ far upstream, it is clear that H_i far upstream can be expressed as a linear function of Z: $H_i = A_i + B_i Z$ where A_i and B_i are constants. Further, $H_i = A_i + B_i Z$ also satisfies (2.12), because of (2.11). It follows therefore, that $H_i = A_i + B_i Z$ throughout the domain. The conditions $Y_0 = 1$ in the fuel stream and $Y_0 = 0$ in the oxidizer stream determine the constants A_i and B_i. Thus, using the definition of H_i, Y_0 and Y_1 may be expressed in terms of Z and T as follows:

$$Y_0 = (T_\infty - T)\frac{m_0 v_0 c_p}{Q} + Z, \tag{2.13}$$

and similarly

$$Y_1 = (T_\infty - T)\frac{m_1 v_1 c_p}{Q} - Z + 1. \tag{2.14}$$

2.2. *Dimensionless variables*

In order to identify suitable dimensionless parameters, it is convenient to express the basic equations in terms of dimensionless variables whose magnitudes are of order unity. Thus, we introduce the dimensionless density and velocity $\varpi = \rho/\rho_\infty$ and $(U, V) = (u/U_\infty, v/U_\infty)$ respectively. An appropriate length scale is the diffusion length k/U_∞, so that we introduce the dimensionless coordinates $(X, Y) = (xU_\infty/k, yU_\infty/k)$. A suitable temperature scale is not T_∞ but some measure of the temperature change across the flame. Clearly, the maximum temperature is reached just behind the flame front along the stoichiometric line, where the combustion is complete (there is neither fuel nor oxidizer left in the product stream). This 'adiabatic flame temperature', T_s, is obtained by putting $Z = Z_s = 1/(1 + r)$ and $Y_0 = 0$ in (2.13)

$$T_s = T_\infty + \frac{Q}{m_0 v_0 c_p}\frac{1}{1 + r} = T_\infty + \frac{Q}{(m_0 v_0 + m_1 v_1)c_p}. \tag{2.15}$$

The dimensionless parameter

$$\alpha \equiv \frac{T_s - T_\infty}{T_s} = \left[1 + \frac{(m_0 v_0 + m_1 v_1)c_p T_\infty}{Q}\right]^{-1} \tag{2.16}$$

characterizes the temperature rise, or equivalently, the amount of heat released in the flame. Further, we introduce the dimensionless temperature, Θ, defined as

$$\Theta = \frac{T - T_\infty}{T_s - T_\infty}. \tag{2.17}$$

A second important dimensionless parameter is the Zeldovich number, β, defined as (Liñán & Williams 1993)

$$\beta \equiv \alpha \frac{T_a}{T_s}, \tag{2.18}$$

a measure of the sensitivity of the reaction rate (2.5) to temperature. In terms of these dimensionless variables, (2.8) may be written as

$$\varpi\left(U\frac{\partial\Theta}{\partial X} + V\frac{\partial\Theta}{\partial Y}\right) = \frac{\partial^2\Theta}{\partial X^2} + \frac{\partial^2\Theta}{\partial Y^2} + \lambda\varpi^{v_0 + v_1}\Sigma(Z/Z_s, \Theta)\exp\left[-\frac{\beta(1 - \Theta)}{1 - \alpha(1 - \Theta)}\right] \tag{2.19}$$

where Σ is defined by

$$\Sigma(x, y) \equiv (x - y)^{v_0}[(1 - x) + r(1 - y)]^{v_1}, \tag{2.20}$$

and λ is defined by

$$\lambda = \frac{kQA}{c_p T_s \alpha}\frac{\rho_\infty^{v_0 + v_1 - 1}}{(1 + r)^{v_0 + v_1}}\exp(-\beta/\alpha)\frac{1}{U_\infty^2}. \tag{2.21}$$

The equation for the mixture fraction Z, (2.11), becomes

$$\varpi\left(U\frac{\partial Z}{\partial X} + V\frac{\partial Z}{\partial Y}\right) = \frac{\partial^2 Z}{\partial X^2} + \frac{\partial^2 Z}{\partial Y^2} \tag{2.22}$$

and the density is related to the temperature through (2.7), which may be re-expressed in dimensionless form as

$$\varpi = \frac{1 - \alpha}{1 - \alpha(1 - \Theta)}. \tag{2.23}$$

Variations in density due to temperature changes modify the velocity field through the continuity equation, (2.6), which may be written in dimensionless variables as

$$\frac{\partial(\varpi U)}{\partial X} + \frac{\partial(\varpi V)}{\partial Y} = 0. \tag{2.24}$$

Equations (2.19), (2.22), (2.23) and (2.24) are coupled equations for the temperature, mixture fraction and density fields. These need to be complemented with two equations for the X- and Y-components of momentum and appropriate boundary conditions, and these will be discussed later in §4. In writing these equations the problem has been assumed steady and two-dimensional.

2.3. *Low-heat-release approximation*

The reduced set of equations (2.19), (2.22), (2.23), (2.24) are still complex and not amenable to analytical solution. We will therefore introduce the further approximation of 'low heat release', by which we mean $\alpha \ll 1$. In this approximation, the density variations are sufficiently weak that we may take $\varpi = 1$ in (2.19), (2.22), (2.24). Therefore, the velocity (U, V) decouples in this approximation from the density, so that for the velocity field we have the trivial solution $U = 1$ and $V = 0$. Equations for the temperature (2.19) and mixture fraction (2.22) then reduce to

$$\frac{\partial \Theta}{\partial X} = \frac{\partial^2 \Theta}{\partial X^2} + \frac{\partial^2 \Theta}{\partial Y^2} + \lambda \Sigma(Z/Z_s, \Theta) \exp\left[-\beta(1 - \Theta)\right] \tag{2.25}$$

and

$$\frac{\partial Z}{\partial X} = \frac{\partial^2 Z}{\partial X^2} + \frac{\partial^2 Z}{\partial Y^2}. \tag{2.26}$$

Equation (2.26) is elliptic. However, if Z varies much more rapidly in the direction perpendicular to the flow (Y-direction) than in the direction of the flow (X-direction) as in a slowly spreading mixing layer, the first term on the right-hand side may be neglected. The equation then becomes hyperbolic and its solution is determined uniquely once the mixture-fraction profile far upstream, $Z(-\infty, Y)$ is specified. If the spatial extent of the flame (characterized by the flame thickness) is much smaller than the thickness of the mixing layer, one may assume the mixture fraction profile to be linear in the neighbourhood of the flame, $Z = A + BY$ (A and B are constants). The linear profile also happens to be an exact solution of (2.26), though it does not satisfy the lateral boundary conditions $Z \to 0$ or 1 as $Y \to \pm\infty$. In this paper we will assume the linear profile for $Z(Y)$.

Since the gases far upstream are at a uniform temperature, we have the boundary condition

$$\Theta(-\infty, Y) = 0. \tag{2.27}$$

Far downstream of the flame, at a fixed value of Y, the deficient component (fuel or oxidizer) is completely consumed; thus, $Y_1(\infty, Y) = 0$ for $Y \geqslant 0$, and, $Y_0(\infty, Y) = 0$ for $Y \leqslant 0$. These conditions can be expressed in terms of the dimensionless temperature,

Θ, by using (2.13), (2.14), and (2.17) :

$$\Theta(\infty, Y) = \begin{cases} \dfrac{1-Z}{1-Z_s} & \text{if } Y \geqslant 0 \\[2mm] Z/Z_s & \text{if } Y \leqslant 0. \end{cases} \tag{2.28}$$

The elliptic differential equation (2.25) with the prescribed values at the boundaries of the domain define an eigenvalue problem for the parameter λ on the right-hand side of (2.25). Thus, the flame speed, which is related to λ through equation (2.21), is to be determined as an eigenvalue of the problem.†

The modification of the flow field due to heat release has important consequences for the structure and propagation of triple flames (Ruetsch *et al.* 1995). The lowest-order equations (2.25) and (2.26) will not show these effects since the modification of the flow field by the flame has been neglected. Such effects can however be included by going to the next order in the asymptotic expansion with respect to the small parameter α; (2.25) and (2.26) are the lowest-order equations resulting from such an expansion. The corrected density may be obtained from (2.23) by expanding in the small parameter α:

$$\varpi = 1 - \alpha\Theta + O(\alpha^2), \tag{2.29}$$

where Θ denotes the solution of the pair of equations (2.25) and (2.26). On substituting (2.29) in (2.24) and retaining only terms that are linear in α, we obtain the following equation for the correction, $(\delta U, \delta V)$, to the velocity at leading order:

$$\frac{\partial(\delta U)}{\partial X} + \frac{\partial(\delta V)}{\partial Y} = \alpha\frac{\partial\Theta}{\partial X}. \tag{2.30}$$

We will return to (2.29) and (2.30) in §4.

3. Activation-energy asymptotics

The Zeldovich parameter β defined by (2.18) is often moderately large ($\beta \sim 10$ or larger) for many processes of practical interest. It is therefore useful to study the basic equations describing flames in the asymptotic limit of $\beta \to \infty$. This limit is known as 'activation-energy asymptotics' (AEA). It is clear from (2.25) that, in the limit $\beta \to \infty$, the source term vanishes, except in the immediate vicinity of the flame front ($\Theta = 1$). Since the integrated reaction rate must be finite, it is clear that the source term must become singular in this limit at the flame front ($\Theta = 1$), indicating that the limit must be treated as a singular perturbation problem (Van-Dyke 1975). Such solutions for the case of a premixed plane flame are well known (Liñán & Williams 1993).

The AEA analysis was first applied to the triple-flame problem by Dold (1989). In addition to the assumptions of low heat release ($\alpha \ll 1$) and large Zeldovich number ($\beta \gg 1$), Dold assumed that the mixture fraction gradient at the flame was weak, specifically, $\beta(\partial Z/\partial Y) \ll 1$. The curvature of the flame front is controlled by the quantity $\beta(\partial Z/\partial Y)$, which for the general triple-flame problem is of order unity. When $\beta(\partial Z/\partial Y) = 0$, the triple flame reduces to a planar flame whereas in the opposite limit of $\beta(\partial Z/\partial Y) \to \infty$, the flame loses the 'triple-flame' character composed of two partially premixed branches and a trailing diffusion flame. Instead, the partially premixed branches degenerate into a geometrical point. The analysis of Dold describes a weakly curved triple flame which allows a simplified description. The

---

† This formulation gives rise to the 'cold boundary difficulty', a discussion of which may be found in Liñán & Williams (1993) and other standard treatises on combustion.

principal outcome of the analysis was the flame speed and the equation describing the shape of the curved flame front. The above results were subsequently extended by Hartley & Dold (1991) to the generic case, $\beta(\partial Z/\partial Y) \sim O(1)$. However, because of the difficulty in solving the equation for the temperature field in a 'free boundary' type problem (the curved flame front must be determined self-consistently as part of the solution) the flame speed could not be obtained as a closed form analytical expression, but had to be deduced by numerically solving an integral equation.

The work of Dold and Hartley & Dold discussed above does not take into account any effects of density changes due to heat release. The main qualitative effect of heat-release-induced density changes in triple flames have been described by Ruetsch *et al.* (1995), through a careful physical analysis of data obtained by direct numerical simulation of the full set of compressible equations describing the triple flame. It was shown that when heat release effects are included, the associated density changes cause the stream lines of the flow to diverge ahead of the flame tip, causing a reduction in the local flow speed. To stabilize the triple flame, the upstream speed must increase, that is the triple flame moves faster. Further, since the mixture fraction $Z(X, Y)$ is advected like a passive scalar, the mixture fraction gradient just ahead of the flame is reduced, resulting in a further increase in the flame speed due to decreased curvature. Except in situations where the reactants are diluted by an inert component, the value of α is quite large ($\alpha \sim 0.8$), so that the heat release effect plays a dominant role in determining the flame speed.

The objective of the present study is to extend the work of Dold and Hartley & Dold discussed above to include some of the effects of heat release. Our strategy will be to treat density changes due to heat release as a small perturbation to the constant-density solution. To do this we first derive a solution to the constant-density case that is considerably simpler than that presented by Hartley & Dold, by invoking the 'parabolic flame path approximation' discussed in §3.1.

In order to avoid unnecessarily long algebraic calculations, we will, from now on, assume that $v_0 = v_1 = v$ and $m_0 = m_1 = m$. This ensures that the triple flame is symmetric with respect to the centreline. Further, we will assume a linear mixture fraction profile:

$$Z(X, Y) = \tfrac{1}{2}[1 + \mu Y].\tag{3.1}$$

The μ so defined is the dimensionless mixture fraction gradient.

3.1. *Solution in parabolic-cylinder coordinates*

In the limit of large β, the source term on the right of (2.25) may be neglected as exponentially small, except in a thin reaction zone, the 'flame front'. The solution is therefore in two parts: an 'outer solution' valid everywhere except in the immediate neighbourhood of the flame front, and an 'inner solution' for the reaction zone that smoothly connects the two branches (the one in front and the one behind the flame) of the outer solution. Within this approximation of the infinitesimally small reaction zone, the temperature just behind the flame front may be obtained by setting $Y_1 = 0$ (in the fuel stream, $Y > 0$) or $Y_0 = 0$ (in the oxidizer stream, $Y < 0$) in (2.13) and (2.14), since the component that is deficient is completely consumed. We therefore obtain, using (2.17) and (2.15),

$$\Theta = 1 - \mu|Y|\tag{3.2}$$

just behind the flame surface. Therefore, the reaction rate along the flame front varies as $\exp[-\beta\mu|Y|]$, so that, in taking the limit $\beta \to \infty$, we must assume the scaling $\mu \sim 1/\beta$ in order to obtain a well-defined triple flame. The regimes $\beta\mu \gg 1$

correspond to degenerate triple flames that may have negative propagation speeds (Dold 1994); these will not be discussed in the present paper. With this scaling, the effective lateral extent of the reaction zone is $|Y| \sim 1$. It should be mentioned here that the assumption of a linear Z-profile is justified, since the domain of validity of that approximation is $|Y| < 1/\mu \sim \beta$ while the reaction zone is effectively confined to some interval $|Y| < R_1$, where $R_1 \sim O(1)$.

In figure 4, the reaction rate of a triple flame is plotted as a function of the horizontal coordinates X and Y (the data are from Ruetsch *et al.* 1995). The exponential fall-off of the reaction rate $\sim \exp[-\beta\mu|Y|]$ is apparent. Since such properties as the flame speed and curvature of a triple flame are controlled primarily by the reaction rate, it seems reasonable to suppose that these properties are determined primarily by the structure of the immediate vicinity of the flame tip. In the neighbourhood of the flame tip, the shape of the reaction zone can be approximated by a parabolic profile in the region $|Y| \ll 1$. However, since $\beta\mu \sim 1$, it is clear that the reactive zone extends to distances $|Y| \sim 1$, so that the parabolic approximation cannot be strictly justified over the entire reactive zone. We will assume as a *heuristic model* that the unknown flame shape $Y = f(X)$ may be replaced by a parabola in the entire reactive zone. We call this the 'parabolic flame path approximation'. Clearly, this is an *ad hoc* approximation not unlike the 'modal truncation' approach used in various nonlinear fluid problems where no satisfactory closure can be found. Nevertheless, we will find that the model gives remarkably accurate results, indicating perhaps that the quantities we are interested in (flame curvature, speed, temperature distribution) are rather insensitive to the precise shape of the premixed branch of the flame.

This approximation allows a considerable reduction in the complexity of the problem since the 'free boundary' of the flame front can now be regarded as known, except for a single parameter (the flame curvature) which must be self-consistently determined. The essential difference between our treatment and that of Hartley and Dold described earlier is that we exploit this parabolic representation to achieve a solution that is analytically much simpler and yet almost identical in accuracy, though, unlike Hartley and Dold we employ an *ad hoc* approximation of the flame path by a parabola.

Since the flame front is a parabola in our model, it is useful to introduce parabolic-cylinder coordinates defined by

$$X = \tfrac{1}{2}[\xi^2 + \eta_0^2 - \eta^2], \tag{3.3}$$

$$Y = \xi\eta. \tag{3.4}$$

The lines of constant ξ and η are both parabolas (or surfaces of parabolic cylinders if viewed in three dimensions) and the two families of curves intersect each other at right angles. We adopt the convention that the parabola $\eta = \eta_0$ is the one that defines the flame surface, so that the flame surface is defined in Cartesian coordinates by the equation $Y^2 = 2\eta_0^2 X$.

3.1.1. *The outer solution*

For the 'outer solution' the source term on the right-hand side of (2.25) may be dropped so that we need to solve

$$\frac{\partial\Theta}{\partial X} = \frac{\partial^2\Theta}{\partial X^2} + \frac{\partial^2\Theta}{\partial Y^2}. \tag{3.5}$$

The first-derivative term in (3.5) may be eliminated through the substitution

$$\Theta = \exp{(X/2)}F, \tag{3.6}$$

which gives for F the equation

$$\frac{\partial^2 F}{\partial X^2} + \frac{\partial^2 F}{\partial Y^2} - \frac{F}{4} = 0. \tag{3.7}$$

On transforming to parabolic-cylinder coordinates defined by (3.3) and (3.4), (3.7) becomes

$$\frac{\partial^2 F}{\partial \xi^2} + \frac{\partial^2 F}{\partial \eta^2} - \tfrac{1}{4}(\xi^2 + \eta^2)F = 0. \tag{3.8}$$

Equation (3.8) admits separable solutions of the form $F(\xi, \eta) = M(\xi)N(\eta)$ where $M(\xi)$ and $N(\eta)$ satisfy

$$\frac{\mathrm{d}^2 M}{\mathrm{d}\xi^2} + \left(p - \frac{\xi^2}{4}\right)M(\xi) = 0 \tag{3.9}$$

and

$$\frac{\mathrm{d}^2 N}{\mathrm{d}\eta^2} + \left(-p - \frac{\eta^2}{4}\right)N(\eta) = 0 \tag{3.10}$$

respectively. Equation (3.9) is simply the Schrödinger equation for the harmonic oscillator in quantum mechanics, the solution to which is well known (Cohen-Tannoudji, Dieu & Laloe 1977). The requirement of finiteness in the limit $|\xi| \to \infty$ results in the 'quantization condition'

$$p = n + \tfrac{1}{2}, \tag{3.11}$$

where $n = 0, 1, 2, \ldots$, and the eigenfunction corresponding to the eigenvalue n is given by

$$M(\xi) = M_n(\xi) = \exp{(-\xi^2/4)}H_n(\xi), \tag{3.12}$$

$H_n(\xi)$ being the Hermite polynomial of order n. The solutions to (3.10) have different analytical forms in front of ($\eta > \eta_0$) and behind ($\eta < \eta_0$) the curved flame front.

Ahead of the premixed flame (preheat zone)

In the region in front of the premixed flame front ($\eta > \eta_0$), known as the 'preheat zone', the fuel and oxidizer are heated by thermal conduction from the reaction zone. Two linearly independent solutions of (3.10) are $U(n+1/2, \eta)$ and $V(n+1/2, \eta)$, where $U(a, z)$ and $V(a, z)$ are parabolic cylinder functions (Abramowitz & Stegun 1970) that have the following asymptotic representation for large values of z:

$$U(a, z) \sim \exp{(-z^2/4)}z^{-a-1/2}\left\{1 - \frac{(a + 1/2)(a + 3/2)}{2z^2} + \cdots\right\}, \tag{3.13}$$

$$V(a, z) \sim \sqrt{\frac{2}{\pi}} \exp{(z^2/4)}z^{a-1/2}\left\{1 + \frac{(a - 1/2)(a - 3/2)}{2z^2} + \cdots\right\}. \tag{3.14}$$

The solution $V(n + 1/2, \eta) \sim \sqrt{2/\pi} \exp{(\eta^2/4)}\eta^n$ gives $\Theta = \exp{(X/2)}F \sim \eta^n$. Since only solutions that satisfy $\Theta \to 0$ as $\eta \to \infty$ are acceptable, we have

$$N_n(\eta) = U(n + 1/2, \eta). \tag{3.15}$$

A general solution for Θ may be constructed by linear superposition:

$$\Theta(\xi,\eta) = \exp\left[(\eta_0^2 - \eta^2)/4\right] \sum_{n=0}^{\infty} a_n H_n(\xi) U(n + 1/2, \eta), \tag{3.16}$$

where use has been made of (3.3), (3.6), (3.12) and (3.15). Since the temperature just behind the partially premixed front is given by (3.2) and since the temperature must be continuous across the flame surface, we have the boundary condition

$$\Theta(\xi,\eta_0) = 1 - \mu\eta_0|\xi|. \tag{3.17}$$

The requirement that (3.16) reduce to (3.17) on the flame front $\eta = \eta_0$ determines the coefficients a_n as follows:

$$a_n = \frac{\displaystyle\int_{-\infty}^{+\infty} \{1 - \mu\eta_0|\xi|\} H_n(\xi) \exp(-\xi^2)\, \mathrm{d}\xi}{2^n n! \sqrt{\pi} U(n + 1/2, \eta_0)}. \tag{3.18}$$

Clearly, only even coefficients are non-zero. Note that, since $\mu = B/\beta \sim O(1/\beta)$, $a_n \sim O(1/\beta)$ for all n except $n = 0$. Thus, replacing the parabolic cylinder function $U(1/2,\eta)$ by its expression in terms of the complementary error function (Abramowitz & Stegun 1970) gives

$$\Theta^{(0)} = \frac{\mathrm{erfc}(\eta/\sqrt{2})}{\mathrm{erfc}(\eta_0/\sqrt{2})} + O(1/\beta). \tag{3.19}$$

Behind the premixed flame

Behind the partially premixed flame front, the X-axis is a line of discontinuity of the first derivative $(\partial\Theta/\partial Y)$, since the diffusion flame is a heat source. Along the diffusion flame, the source term in (2.25) is almost exactly balanced (Burke & Schumann 1928) by the lateral diffusion of heat represented by the term $\partial^2\Theta/\partial Y^2$, so that X-derivatives are vanishingly small. Thus, the appropriate boundary condition along the line $Y = 0$ $(X > 0)$ is

$$\Theta(X,0) = 1. \tag{3.20}$$

It is easily verified that $\Theta = 1 - \mu Y$ satisfies (3.5) in the region defined by $X > 0$ and $0 < Y < \sqrt{(2\eta_0^2 X)}$ subject to the boundary conditions (3.2) and (3.20). It is therefore the unique outer solution in the region behind the partially premixed front with $Y > 0$. Since the solution must be symmetric with respect to the Y-axis, the general result, valid for any sign of Y is

$$\Theta(X,Y) = 1 - \mu|Y|, \tag{3.21}$$

for $X > 0$ and $Y^2 < 2\eta_0^2 X$. Since $\mu = B/\beta \sim O(1/\beta)$, the following approximate form may be used behind the premixed front:

$$\Theta(X,Y) = 1 + O(1/\beta). \tag{3.22}$$

3.1.2. *The inner solution and asymptotic matching*

We now determine the solution to (2.25) in the immediate vicinity of the reaction zone. The analysis that follows closely parallels the AEA solution for the planar premixed flame (Liñán & Williams 1993). Equation (2.25) may be written in parabolic-cylinder coordinates as follows:

$$\xi\frac{\partial\Theta}{\partial\xi} - \eta\frac{\partial\Theta}{\partial\eta} = \frac{\partial^2\Theta}{\partial\xi^2} + \frac{\partial^2\Theta}{\partial\eta^2} + \lambda(\xi^2 + \eta^2)F(1 + \mu\xi\eta, \Theta)\exp[-\beta(1 - \Theta)]. \tag{3.23}$$

The differential element of length orthogonal to the flame front at some location (ξ_0, η_0) on the flame surface is $\mathrm{d}s = \sqrt{\mathrm{d}X^2 + \mathrm{d}Y^2} = \sqrt{\eta_0^2 + \xi_0^2}\, \mathrm{d}\eta$. Since the flame thickness $\sim 1/\beta$, an appropriate inner variable is $\tau = \beta(\eta - \eta_0)$. We also define the new variable θ which is the deviation of the temperature from that on the flame surface scaled to order unity:

$$\Theta = 1 - \mu\eta_0|\xi| - \frac{\theta}{\beta}. \tag{3.24}$$

We now rewrite (3.23) in terms of these scaled variables, expand $\theta(\xi, \tau)$ in an asymptotic series in $1/\beta$, and retain only leading-order terms to derive

$$\theta_{\tau\tau} = \Lambda_0(\xi^2 + \eta_0^2)\theta^v(\theta + 2B\eta_0|\xi|)^v \exp(-\theta)\exp(-B\eta_0|\xi|), \tag{3.25}$$

where $B \equiv \beta\mu \sim O(1)$ and we have expanded the eigenvalue λ as $\lambda = \beta^{2v+1}(\Lambda_0 + \beta^{-1}\Lambda_1 + \cdots)$. Equation (3.25) can be integrated using the boundary condition $\theta_\tau(\tau = 0) = 0$ to give

$$\theta_\tau^2(\tau \to +\infty) = 2\Lambda_0(\xi^2 + \eta_0^2)\exp(-B\eta_0|\xi|)\mathscr{F}_v(2B\eta_0|\xi|), \tag{3.26}$$

where the function $\mathscr{F}_v$ is defined as

$$\mathscr{F}_v(\alpha) = \int_0^\infty \theta^v(\theta + \alpha)^v \exp(-\theta)\, \mathrm{d}\theta. \tag{3.27}$$

To determine the eigenvalue Λ_0 we now enforce the asymptotic matching condition

$$\Theta_\eta(\xi, \eta \to \eta_0) = -\theta_\tau(\xi, \tau \to \infty), \tag{3.28}$$

where the Θ on the left-hand side refers to the outer solution and the θ on the right-hand side refers to the inner solution.

To determine the left-hand side of (3.28) we first note that since $\mu = B/\beta \sim 1/\beta$, (3.18) may be written as

$$a_n = \frac{\delta_{n,0}}{U(1/2, \eta_0)} + O(1/\beta), \tag{3.29}$$

where $\delta_{n,0}$ is the Kronecker delta symbol. Using known (Abramowitz & Stegun 1970) recursion relations for the parabolic cylinder function U, we have

$$\Theta_\eta(\xi, \eta_0) = -\sum_{n=0}^\infty a_n U(n - 1/2, \eta_0)H_n(\xi) = -\frac{U(-1/2, \eta_0)}{U(1/2, \eta_0)} + O(1/\beta). \tag{3.30}$$

The functions $U(\pm 1/2, z)$ can be expressed (Abramowitz & Stegun 1970) in terms of the exponential and the complementary error function erfc, so that (3.28) may be written using (3.30) and (3.26), retaining only lowest-order terms in $1/\beta$, as

$$\frac{U(-1/2, \eta_0)}{U(1/2, \eta_0)} \equiv \sqrt{\frac{2}{\pi}} \frac{\exp(-\eta_0^2/2)}{\mathrm{erfc}(\eta_0/\sqrt{2})} = \left[2\Lambda_0(\xi^2 + \eta_0^2)\exp(-B\eta_0|\xi|)\mathscr{F}_v(2B\eta_0|\xi|)\right]^{1/2}. \tag{3.31}$$

In order that the inner and outer solutions match smoothly over the entire flame path, the condition (3.31) should hold for any value of ξ. If we expand the right-hand side in a Taylor series in ξ and enforce the equality at each order, we obtain an infinite number of equations to determine just two free parameters, Λ_0 and η_0. The problem is over constrained because the outer solution used in its derivation invokes the approximation that the flame path is a parabola which is valid only locally near

$\xi = 0$. Thus, in order to be consistent, we must enforce (3.31) only up to second-order terms in ξ. Equating coefficients of the term ξ^0 in (3.31) we get

$$\sqrt{2\Lambda_0 \Gamma(2\nu + 1)} = \sqrt{\frac{2}{\pi}} \frac{\exp(-\eta_0^2/2)}{\eta_0 \operatorname{erfc}(\eta_0/\sqrt{2})} \qquad (3.32)$$

where Γ is the Gamma-function. The linear term on the right-hand side of (3.31) is identically zero. Equating the coefficients of the quadratic term ξ^2, we obtain

$$\eta_0 = \frac{[4\nu - 2]^{1/4}}{\sqrt{B}}. \qquad (3.33)$$

In the limit $\mu \to 0$ with β fixed, $B \to 0$, so that (3.33) implies $\eta_0 \to \infty$, corresponding to a stoichiometric plane flame with the flame surface given by $X = Y^2/(2\eta_0^2) = 0$. Using the asymptotic representation (Abramowitz & Stegun 1970)

$$\operatorname{erfc}(x) \sim \frac{1}{\sqrt{\pi}} \frac{\exp(-x^2)}{x} \qquad (3.34)$$

valid for large x, we have

$$\Lambda_0 = \frac{1}{2\Gamma(2\nu + 1)}. \qquad (3.35)$$

Further, since $\Lambda_0 = \lambda/\beta^{2\nu+1} + O(1/\beta)$, the last equation may also be written as

$$\lambda = \frac{\beta^{2\nu+1}}{2\Gamma(2\nu + 1)} \qquad (3.36)$$

at leading order in $1/\beta$. Equivalently, using the definition (2.21) of λ, we may rewrite it in terms of physical variables:

$$U_\infty = U_\infty^S = \left[\frac{2mkA\nu\Gamma(2\nu + 1)}{\beta^{2\nu+1}} \left(\frac{\rho_\infty}{2} \right)^{2\nu-1} \exp(-\beta/\alpha) \right]^{1/2}, \qquad (3.37)$$

the well known (Liñán & Williams 1993) expression for the speed of a stoichiometric plane flame. In deriving (3.37) we combined (2.15) and (2.16) to express the heat released per reaction as $Q = 2m\nu c_p \alpha T_s$.

Using (3.37) and (2.21), equations (3.32) and (3.33) may also be rewritten as follows:

$$\frac{U_\infty}{U_\infty^S} = \sqrt{\pi/2}\, \eta_0 \exp(\eta_0^2/2) \operatorname{erfc}(\eta_0/\sqrt{2}), \qquad (3.38)$$

$$\frac{k}{U_\infty^S} \frac{1}{Z_s} \frac{\partial Z}{\partial y} = \frac{\sqrt{4\nu - 2}}{\beta\eta_0^2} \frac{U_\infty}{U_\infty^S}, \qquad (3.39)$$

$$\frac{k}{U_\infty^S} \kappa = \frac{1}{\eta_0^2} \frac{U_\infty}{U_\infty^S}. \qquad (3.40)$$

Here U_∞ is the speed of the triple flame in physical units, $\kappa \equiv \mathrm{d}^2 x/\mathrm{d}y^2$ is the flame curvature, $\partial Z/\partial y$ is the fuel mixture fraction gradient in dimensional units, $Z_s = Z(0) = 1/2$ is the stoichiometric mixture fraction, and, U_∞^S is the stoichiometric planar flame speed given by (3.37). Equations (3.38)–(3.40) determine in parametric form (with parameter η_0) the triple flame speed and curvature as a function of the imposed mixture fraction gradient. It should be noted that the Zeldovich number, β, enters into this equation only in the combination $\beta(\partial Z/\partial y)$. These equations are

our principal results in the low-heat-release case, and are discussed further in the following section.

A quantity often of interest is the integrated heat release in the flame. The jump in the normal component of $\nabla \Theta$ across the premixed branch, $\Omega_p(\xi)$, and, across the diffusion branch, $\Omega_d(\xi)$, are proportional to the integrated reaction rates (or heat release) across the appropriate branches. We have, from (3.30) and (3.21),

$$\Omega_p(\xi) = \frac{1}{\sqrt{\xi^2 + \eta_0^2}} \left[\sum_{n=0}^{\infty} a_n H_n(\xi) U(n - 1/2, \eta_0) - \mu|\xi| \right] \tag{3.41}$$

and

$$\Omega_d(\xi) = 2\mu. \tag{3.42}$$

The reaction rate integrated in the y-direction is a quantity more easily evaluated from numerical simulation data. From purely geometrical considerations, the following expression may be written down for the y-integrated reaction rate normalized by the reaction rate integrated across the diffusion branch:

$$\Omega_Y(X) = \begin{cases} 1 + \dfrac{\sqrt{\xi^2 + \eta_0^2}}{2\mu|\xi|} \Omega_p(\xi) & \text{if } X \geqslant 0 \\ 0 & \text{if } X < 0, \end{cases} \tag{3.43}$$

where $\xi = \pm\sqrt{2X}$. This expression is used in the next section for comparison with data from numerical simulations.

3.2. *Discussion of solution*

The normalized flame speed determined as a function of the dimensionless mixture fraction gradient $(k/U_\infty^S)Z_s^{-1}(\partial Z/\partial y)$ from the pair of equations (3.38) and (3.39) is shown in figure 5 as a solid line. The data from figure 8(*b*) of Hartley & Dold (1991) are shown by the symbols. The Zeldovich parameter $\beta = 7.5$. The two results are in excellent agreement. Our result differs from that of Hartley & Dold (1991) in that we have an explicit analytic expression, defined by (3.38) and (3.39), for the flame speed, whereas Hartley & Dold generate the data in their figure 8(*b*) by numerically solving an integral equation (equation(26) in their paper). However, they do provide analytic expressions in the two limits $\mu\beta \ll 1$ and $\mu\beta \gg 1$. Further, our outer solution for the temperature field defined by (3.16) and (3.21) is obtained explicitly whereas in Hartley & Dold (1991) it is only given implicitly as the solution of an integral equation which needs to be solved numerically. This simplification, however, has been made at the expense of rigour. The theory of Hartley & Dold is the rigorous asymptotic ($\beta \to \infty$) theory whereas our results invoke the additional *ad hoc* approximation of the parabolic flame path. The close agreement between these two sets of data is quite remarkable.

We now present comparisons between our theoretical results and numerical simulations of (2.25). The numerical methods for doing this have been described in detail elsewhere (Lele 1992; Poinsot & Lele 1992). For computational efficiency we choose a fully incompressible two-dimensional code. The Z-profile at the inlet is chosen as fully linear: $Z = (1 + \mu Y)/2$. Throughout this section the Zeldovich parameter is held fixed at $\beta = 15$, while the normalized mixture fraction gradient $(k/U_\infty^S)Z_s^{-1}(\partial Z/\partial y)$ is varied.

In figure 6 we show the dependence of the normalized flame speed U_∞/U_∞^S on the dimensionless mixture fraction gradient $(k/U_\infty^S)Z_s^{-1}(\partial Z/\partial y)$. The solid line is
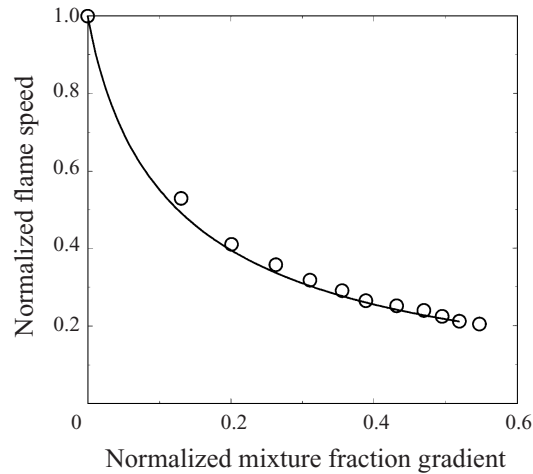
FIGURE 5. Normalized flame speed as a function of the dimensionless MFG according to equations (3.38) and (3.39) (solid line) and according to Hartley & Dold (1991) (symbols) for $\beta = 7.5$.
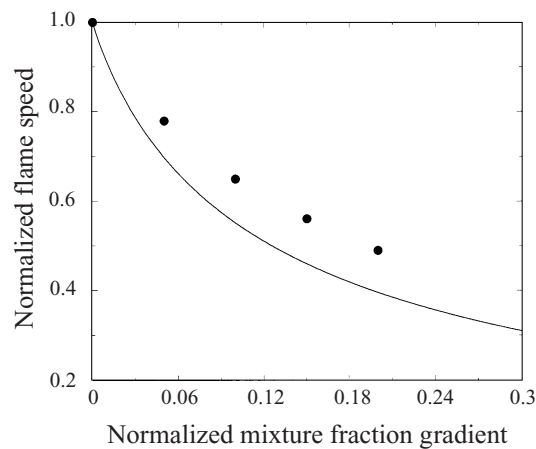

FIGURE 6. The normalized speed of the triple flame as obtained from numerical simulation (symbols), and, as given by equations (3.38) and (3.39) (solid line) as a function of the dimensionless MFG.

obtained from (3.38) and (3.39) and the symbols are the numerical data. The theory correctly predicts the qualitative nature of the variation of the flame speed; however, the theoretical values are too low by about 10%. This is consistent with asymptotic theory since the term next to leading order in the expansion of the flame speed is expected to be smaller by a factor of $1/\beta \approx 0.07$ when $\beta = 15$. This is also consistent with past experience since comparisons between computations and AEA for planar premixed flames give similar levels of accuracy (Peters 1982).

The contours for the reaction rate are shown in figure 7 for a value of the dimensionless mixture fraction gradient of 0.1. Superposed on them is the parabola with curvature given by the theoretical formula (3.40). The correspondence between the true reaction path (flame surface) and the theoretically determined parabola is reasonably good.

Figure 8 shows the theoretical value for the relative temperature change $\Theta(X, 0)$ along the X-axis as provided by (3.16) and (3.21). The agreement between theory and
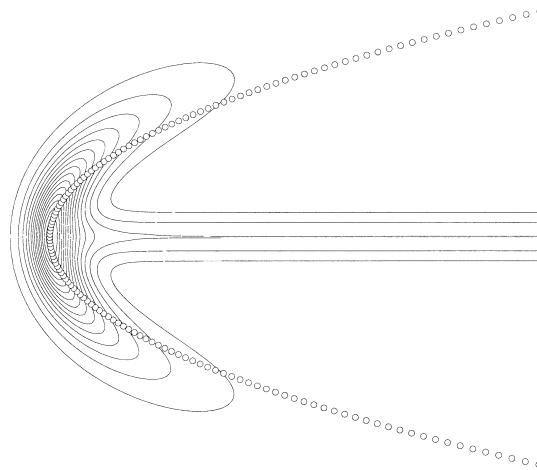
FIGURE 7. Isocontours of reaction rate (solid line) from numerical simulations superposed on theoretical reaction path (symbols) with curvature obtained from (3.40). The dimensionless MFG is 0.1.
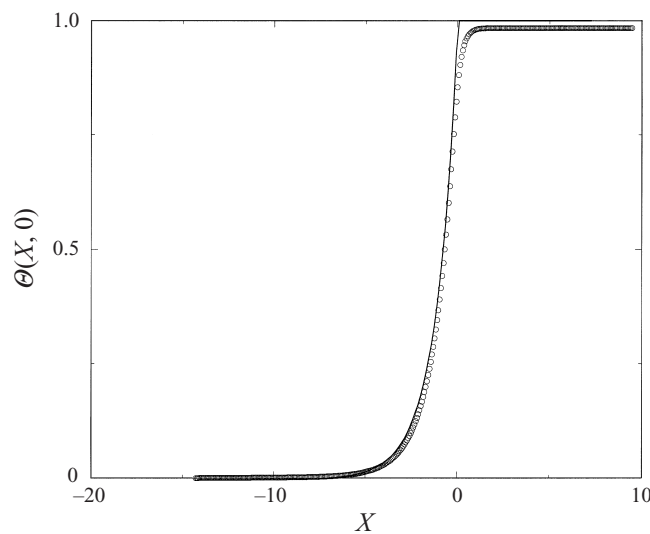

FIGURE 8. The temperature profile $\Theta(X, 0)$ as obtained from numerical simulations (symbols), and, as given by equation (3.16) (solid line) as a function of X. The dimensionless MFG is 0.05.

simulation is excellent. The value of Θ behind the flame in the simulation is slightly less than unity because of the existence of an 'inner solution' for the diffusion branch the structure of which is well known (Liñán & Crespo 1976). The effect of this inner solution is to allow some leakage of fuel and oxidizer across the stoichiometric line so that the maximum temperature reached is less than the adiabatic value, $\Theta = 1$.

Figure 9 shows the temperature along the Y-axis, $\Theta(0, Y)$. The definition of the triple point is not without ambiguity in the case of the numerical simulation, since, unlike in the theory, the flame thickness is small but finite. The location of the triple point may be associated with the point where the reaction rate is maximum. Alternatively, the point where $\Theta(X, 0)$ first reaches its maximal value could be used. The numerical simulation is therefore represented by two curves one of which (the circles) identifies the triple point (the origin of coordinates) with the maximum
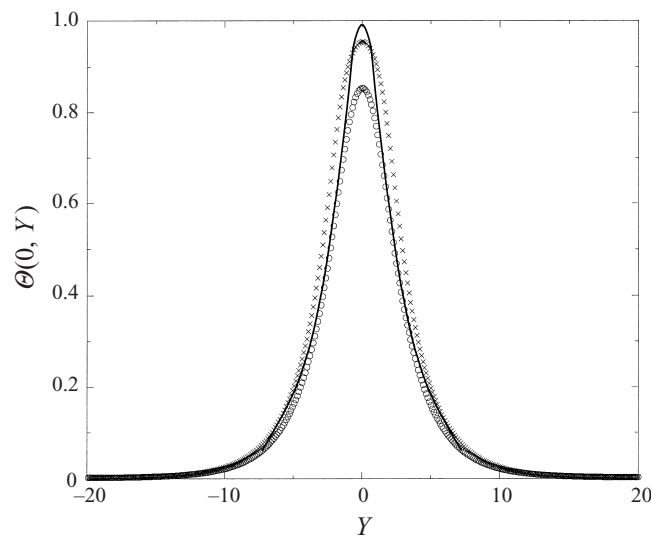
FIGURE 9. The temperature profile $\Theta(0, Y)$ as obtained from numerical simulations (symbols), and, as given by equation (3.16) (solid line) as a function of Y. In the simulations, the flame has finite thickness so the tip of the flame is not uniquely defined. The two types of symbols correspond to two different ways of defining the flame tip (see text). The dimensionless MFG is 0.05.

reaction rate and the other (the crosses) identifies the triple point with the maximum of the temperature. The curves corresponding to these two choices are nevertheless quite close and the agreement with theory is seen to be quite good.

Figure 10 shows the reaction rate integrated in the Y-direction as a function of X, normalized by the integrated reaction rate across the diffusion branch. The theoretical value of this function is given by (3.43) while the corresponding numerical simulation result has been obtained by numerically integrating the reaction rate data in the Y-direction. The correspondence between theory and simulation is seen to be reasonable. The theoretical curve has a $\sim 1/\sqrt{X}$ type integrable singularity at the origin. This is a simple geometrical consequence of integrating in a direction tangential to the flame front of an infinitely thin flame. The slight oscillation of the theoretical curve for $X > 4$ is a numerical artifact of attempting to evaluate the right-hand side of (3.41) by replacing the infinite sum by a finite one. The construction of the outer solution involves representation of the non-smooth 'top-hat' function, (3.17), by an infinite series of Hermite polynomials. Truncation of this series to a finite number of terms during numerical evaluation results in these 'Gibbs-oscillations' as seen in figure 10. The oscillations have been minimized by generating the curve for all integer values of n between 2 and 8 and then taking their average.

4. Effect of heat release

The analyses of Dold (1989) and Hartley & Dold (1991) neglect density changes in the triple flame due to heat release and the consequent modification of the flow field around the triple flame. However, numerical simulation (Ruetsch *et al.* 1995) of the full set of compressible equations (2.1)–(2.6) shows that such density changes due to heat release have important qualitative effects on the structure and propagation speed of a triple flame. As pointed out by Ruetsch *et al.* (1995), the heat released within the curved flame front causes an entropy jump across the flame. The resulting
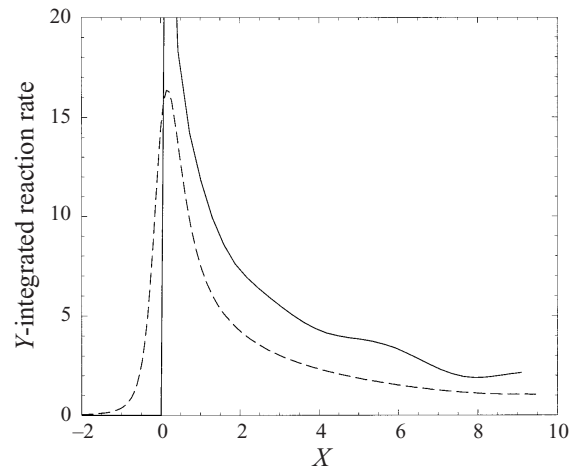
FIGURE 10. The reaction rate integrated over all Y, plotted as a function of X, for theory (solid line) and simulation (dashed line). Normalization is by the reaction rate integrated across the diffusion flame (essentially constant in the simulation and exactly constant in the theory). The dimensionless MFG is 0.1 and $\beta = 15$.

jump in the thermodynamic and flow variables across the flame as determined by the Rankine–Hugoniot conditions for the continuity of mass, momentum and energy lead to an outward deviation of the streamlines in front of the triple flame. The streamlines tend to diverge in front of the flame. There are two important qualitative effects of this streamline divergence as pointed out by Ruetsch *et al.* (1995). First, in a frame in which the flame is stationary, the fluid velocity at the flame tip is less than the upstream value. Since, for equilibrium, the fluid velocity at the tip of the flame must match the stoichiometric burning speed (reduced somewhat by curvature effects) the fluid velocity far upstream must be larger than it would be without this compressibility effect. Thus, in a frame in which the fluid is at rest in the far field, the triple-flame propagation speed is increased by compressibility effects. The other effect of this streamline divergence is that the mixture fraction gradient at the flame tip is reduced compared to its upstream value. This follows since the fuel mixture fraction Z evolves like a passive scalar so that two neighbouring values of Z are pulled apart as they get advected by the fluid (diffusion has an additional smoothing effect but it does not change the qualitative fact that gradients of Z are reduced). As discussed in the previous section, it is the mixture fraction gradient that causes the flame to curve, and curvature enhances heat loss and therefore reduces flame speed. Thus, the reduction of the mixture fraction gradient causes the flame to have less curvature and higher propagation speed than one without such compressibility effects. Another important effect of this reduction of the mixture fraction gradient is that it can enable a triple flame to exist in locations within the flow field where the mixture fraction gradient would otherwise be large enough to cause quenching of a pure diffusion flame (Domingo & Vervisch 1996).

In this section we extend the results of § 3 to include the lowest-order effects of heat release. In § 4.1, § 4.2 and § 4.3 we linearize about the base solution of § 3 to derive the lowest-order perturbation in the uniform flow field. This is then used in § 4.2 and § 4.3 to compute the reduced mixture fraction gradient and the pertubation in the outer solution for the temperature field respectively. The speed and curvature of the triple flame is determined in § 4.4 by matching the new outer solution with the

inner solution. A physical discussion of these results together with comparisons with numerical simulations are presented in §4.5.

4.1. *Flow modification due to heat release*

Variation of temperature across the curved premixed front can lead to vorticity production through the baroclinic mechanism. The equation for the generation of vorticity, $\boldsymbol{\omega} = \omega\hat{\boldsymbol{z}}$ may be written in dimensionless units as

$$\varpi \frac{\mathrm{D}}{\mathrm{D}t}\left(\frac{\boldsymbol{\omega}}{\varpi}\right) = \frac{1}{M^2}\left(\frac{\nabla\varpi \times \nabla p}{\varpi^2}\right). \tag{4.1}$$

Here ϖ is the density normalized by ρ_∞, p is the pressure normalized by p_∞, the vorticity $\boldsymbol{\omega}$ has been normalized by U_∞^2/k and the Mach number is defined as $M = U_\infty/c_s$ where the sound speed c_s may be taken equal to its value far upstream. Variations of pressure and density tangential to the premixed front are due to the gradient of the mixture fraction, so that we have the estimates $(\nabla p/p)_t \sim M^2\mu$ and $(\nabla\rho/\rho)_t \sim \mu$. On the other hand, the variation across the flame front is due to heat release and is controlled by the parameter α, so that $(\nabla p/p)_n \sim M^2\alpha$ and $(\nabla\rho/\rho)_n \sim \alpha$ (the suffix 't' or 'n' indicates tangential or normal component respectively). Therefore, the right-hand side of (4.1) is of the order of $\mu\alpha = B\alpha/\beta$. Since we are concerned with the regime $B \sim O(1)$, $\alpha \ll 1$ and $\beta \gg 1$, baroclinic generation of vorticity may be neglected. In the presence of molecular viscosity a term proportional to $\nabla^2\omega$ must be added to the right-hand side of (4.1). However, this does not change our conclusion regarding the irrotational nature of the flow, since in the absence of rigid boundaries the viscous term is not in itself a source of vorticity but merely serves to diffuse the (negligible) vorticity generated through the baroclinic mechanism. In more realistic combustion models the viscosity can vary across the flame due to temperature changes and this can be an additional source of vorticity. Numerical simulations do show that vorticity is generated by the premixed front, but the magnitude of this vorticity is small as expected. Thus, we may describe the velocity perturbation using a potential $\Psi(X, Y)$ so that

$$U = 1 + \alpha\Psi_X + \cdots, \tag{4.2}$$

$$V = \alpha\Psi_Y + \cdots. \tag{4.3}$$

On substituting the above equations and (2.23) in the continuity equation (2.24), expanding in an asymptotic series in α, we have at the leading order

$$\Psi_{XX} + \Psi_{YY} = \Theta_X^{(0)}, \tag{4.4}$$

where $\Theta^{(0)}$, the leading order term in

$$\Theta = \Theta^{(0)} + \alpha\Theta^{(1)} + \cdots, \tag{4.5}$$

is given by (3.16) and (3.21) outside the inner reaction zone. Since $\mu = B/\beta \sim O(1/\beta)$, we may use the approximation (3.19) and (3.22) for $\Theta^{(0)}$ in (4.4) and after transforming to parabolic-cylinder coordinates, we have

$$\Psi_{\xi\xi} + \Psi_{\eta\eta} = 0 \tag{4.6}$$

behind the premixed front and

$$\Psi_{\xi\xi} + \Psi_{\eta\eta} = \sigma\eta \exp\left(\frac{\eta_0^2 - \eta^2}{2}\right) \tag{4.7}$$

in front of it, where, for brevity,

$$\sigma^{-1} = \sqrt{\pi/2} \, \exp\left(\eta_0^2/2\right) \operatorname{erfc}\left(\eta_0/\sqrt{2}\right). \tag{4.8}$$

The (X, Y)-plane is mapped in (ξ, η)-space onto the half-plane $+\infty > \xi > -\infty$ and $\infty > \eta > 0$. The X-axis is mapped onto the two lines $\xi = 0$ ($\eta > 0$) and $\eta = 0$ ($+\infty > \xi > -\infty$). Symmetry requires that V must vanish on the X-axis, and this translates in (ξ, η)-space to the two conditions

$$\Psi_\xi(0, \eta) = 0, \tag{4.9}$$

$$\Psi_\eta(\xi, 0) = 0 \tag{4.10}$$

($\eta \geqslant 0$ and $+\infty > \xi > -\infty$); the former is satisfied by all solutions that are symmetric in ξ.

The solution to (4.6) and (4.7) subject to the boundary condition (4.9) and the requirement that the velocity perturbation should vanish far upstream is clearly $\Psi(\xi, \eta) = \Psi_0(\eta)$ where

$$\frac{\mathrm{d}^2 \Psi_0}{\mathrm{d}\eta^2} = \sigma\eta \exp\left(\frac{\eta_0^2 - \eta^2}{2}\right) \tag{4.11}$$

for $\eta \geqslant \eta_0$ and

$$\frac{\mathrm{d}^2 \Psi_0}{\mathrm{d}\eta^2} = 0 \tag{4.12}$$

for $\eta_0 > \eta \geqslant 0$. The solution to (4.12) in the region $\eta_0 > \eta \geqslant 0$ subject to the boundary condition $\Psi_0'(0) = 0$ (which follows from (4.10)) is $\Psi_0(\eta) = C$ where C is a constant. Since the velocity potential is determined only up to a constant we may take $C = 0$ without loss of generality. Thus,

$$\Psi_0(\eta) = 0, \tag{4.13}$$

for $\eta_0 \geqslant \eta \geqslant 0$. Since the temperature and hence the density is continuous across the reaction zone, the velocity too must be continuous. Continuity of the velocity and velocity potential across the flame front requires that in the region $\infty > \eta > \eta_0$ we must solve (4.11) with the boundary conditions

$$\Psi_0(\eta_0) = \Psi_0'(\eta_0) = 0. \tag{4.14}$$

The solution is easily found by integration. Thus,

$$\Psi_0(\eta) = \frac{\operatorname{erfc}\left(\eta/\sqrt{2}\right)}{\operatorname{erfc}\left(\eta_0/\sqrt{2}\right)} + \sigma(\eta - \eta_0) - 1 \tag{4.15}$$

for $\eta > \eta_0$ and

$$\Psi_0(\eta) = 0 \tag{4.16}$$

for $\eta \leqslant \eta_0$.

The velocities along the axes $X = 0$ and $Y = 0$ are determined from (4.15) and (4.16) as

$$U(X, 0) = \begin{cases} 1 - \dfrac{\alpha\sigma}{\sqrt{\eta_0^2 - 2X}} \left[1 - \exp(X)\right] & \text{if } X < 0 \\[2mm] 1 & \text{otherwise} \end{cases} \tag{4.17}$$

and

$$V(0, Y) = \frac{\alpha\sigma\xi}{\eta_0^2 + 2\xi^2} \left[1 - \exp\left(-\xi^2/2\right)\right], \tag{4.18}$$

where $Y = \xi\sqrt{\xi^2 + \eta_0^2}$. These results will be compared to numerical simulations in §4.5.

The theoretical result, (4.17), does show the expected decrease in fluid velocity in front of the triple flame. However, upon crossing the flame, the fluid speed rises only to the level of the upstream value. Numerical simulations, however, show that on crossing the flame front, the fluid velocity increases sharply, overshooting the upstream value. It only returns to the upstream value far behind the flame front (see e.g. Ruetsch *et al.* 1995 or figure 14 of this paper). This qualitative behaviour is not correctly predicted by our model. This appears to be due to neglect of order-$1/\beta$ terms in this simplified analysis, which essentially amounts to ignoring the decay of the temperature gradient along the premixed wing of the flame. If the temperature gradient is artifically cut off at $|Y| = 1/\mu$, the overshoot behaviour is recovered.

4.2. *Reduction of the mixture fraction gradient near the flame tip*

It is clear from (4.18) that line elements along the Y-axis get stretched as they are advected towards the flame, reducing the mixture fraction gradient at the flame tip relative to its upstream value. To calculate the amount of this reduction we must compute the perturbation, ζ, in the mixture fraction field due to heat release:

$$Z = \tfrac{1}{2}(1 + \mu Y) + \alpha\zeta + \cdots. \tag{4.19}$$

To find an equation for ζ, we substitute (4.19) in (2.22), expand all dependent variables in asymptotic series in α and drop all terms of order α^2 or higher. This gives

$$\frac{\partial^2\zeta}{\partial X^2} + \frac{\partial^2\zeta}{\partial Y^2} - \frac{\partial\zeta}{\partial X} = \frac{1}{2}\mu\frac{\partial\Psi}{\partial Y}, \tag{4.20}$$

which may be written in parabolic-cylinder coordinates as

$$\frac{\partial^2\zeta}{\partial\xi^2} + \frac{\partial^2\zeta}{\partial\eta^2} - \xi\frac{\partial\zeta}{\partial\xi} + \eta\frac{\partial\zeta}{\partial\eta} = \frac{1}{2}\mu\left(\eta\frac{\partial\Psi}{\partial\xi} + \xi\frac{\partial\Psi}{\partial\eta}\right). \tag{4.21}$$

Since Ψ is a function of η only, $\Psi(\xi,\eta) = \Psi_0(\eta)$ (where $\Psi_0(\eta)$ is given by (4.15) and (4.16)), equation (4.21) is solved by

$$\zeta(\xi,\eta) = \xi F(\eta), \tag{4.22}$$

where $F(\eta)$ satisfies

$$F'' - F + \eta F' = \tfrac{1}{2}\mu\Psi_0'(\eta). \tag{4.23}$$

Behind the premixed flame

Since by symmetry we must have $Z = 1/2$ on the centreline, the following boundary conditions must hold behind the premixed front ($\eta < \eta_0$):

$$\zeta(0,\eta) = 0, \tag{4.24}$$

$$\zeta(\xi,0) = 0, \tag{4.25}$$

which implies

$$F(0) = 0. \tag{4.26}$$

Behind the premixed front $\Psi_0(\eta) = 0$, so that the solution to (4.23) subject to (4.26) is

$$F(\eta) = a\eta, \tag{4.27}$$

where a is a constant yet to be determined.

Ahead of the premixed flame (*preheat zone*)

Using the solution (4.15), in the preheat zone, (4.23) becomes

$$F'' - F + \eta F' = \frac{1}{2}\mu\sigma \left[1 - \exp\left(\frac{\eta_0^2 - \eta^2}{2}\right) \right]. \tag{4.28}$$

Since Z and its first derivatives must be continuous across the flame front, we must solve (4.28) in $\infty > \eta \geqslant \eta_0$ subject to the initial conditions

$$F(\eta_0) = a\eta_0, \tag{4.29}$$

$$F'(\eta_0) = a. \tag{4.30}$$

We seek a solution to (4.28) in the form

$$F(\eta) = \eta f(\eta). \tag{4.31}$$

Then $f(\eta)$ satisfies

$$f'' + \left(\eta + \frac{2}{\eta}\right) f' = \frac{1}{2\eta}\mu\sigma \left[1 - \exp\left(\frac{\eta_0^2 - \eta^2}{2}\right) \right]. \tag{4.32}$$

This is a linear equation in f' and therefore can easily be solved in closed form. The solution subject to the boundary conditions (4.30) is

$$f(\eta) = a + \frac{1}{2}\mu\sigma \left[\left(\frac{1}{\eta_0} - \frac{1}{\eta}\right) - \int_{\eta_0}^{\eta} \mathrm{d}t \left(\frac{1}{2} + \frac{1}{t^2} - \frac{\eta_0^2}{2t^2}\right) \exp\left(\frac{\eta_0^2 - t^2}{2}\right) \right]. \tag{4.33}$$

Clearly, $f(\eta)$ is finite as $\eta \to \infty$, so that

$$f(\eta) \sim A_0 + \frac{A_1}{\eta} + \frac{A_2}{\eta^2} + \cdots, \tag{4.34}$$

where $A_0, A_1, A_2, \ldots$ are constants. Thus,

$$\zeta(\xi, \eta) = \xi\eta f(\eta) = Y \left[A_0 + \frac{A_1}{\eta} + \cdots \right]. \tag{4.35}$$

Now, if we keep Y fixed and let $X \to -\infty$ (or equivalently $\eta \to \infty$) we must have $\zeta \to 0$. Therefore, (4.35) implies that we must require

$$A_0 = f(\infty) = 0. \tag{4.36}$$

The unknown constant a can now be determined by imposing the condition $f(\infty) = 0$ in (4.33) and evaluating the resulting integrals. After some algebra, the result can be written in a remarkably simple form as follows

$$a = \frac{\mu}{4}(\eta_0^2 - \sigma\eta_0 - 1). \tag{4.37}$$

The modified mixture fraction field $Z = (1 + \mu Y)/2 + \alpha\zeta$ along the surface of the premixed flame may be written as

$$Z(\xi, \eta_0) = \tfrac{1}{2}(1 + \mu' Y) \tag{4.38}$$

where $\mu' = \mu + 2\alpha a$. Using (4.37) we have

$$\frac{\mu'}{\mu} = 1 - \frac{\alpha}{2}(1 + \sigma\eta_0 - \eta_0^2) \tag{4.39}$$

which gives the extent of the reduction in the mixture fraction gradient due to heat release.

4.3. *The modified outer solution for the temperature*

The stretching of line elements by the diverging flow in front of the triple flame would also have the effect of altering the temperature field in the preheat zone. To determine this, we must substitute (4.5), (4.2) and (4.3) in (2.19). The leading-order term in α then gives (3.5) for $\Theta^{(0)}$ and at the next order we obtain

$$\Theta_X^{(1)} - \Theta_{XX}^{(1)} - \Theta_{YY}^{(1)} = \Theta^{(0)}\Theta_X^{(0)} - \Psi_X\Theta_X^{(0)} - \Psi_Y\Theta_Y^{(0)} \tag{4.40}$$

everywhere except in the reaction zone. The right-hand side of this equation is known from the leading-order solution. On substituting (3.19), (3.22), (4.15) and (4.16) in the right-hand side, we obtain, after some simplification

$$\xi\Theta_\xi^{(1)} - \eta\Theta_\eta^{(1)} - \Theta_{\xi\xi}^{(1)} - \Theta_{\eta\eta}^{(1)} = \sigma\exp\left(\frac{\eta_0^2 - \eta^2}{2}\right)\left[\frac{\eta\,\mathrm{erfc}\,(\eta/\sqrt{2})}{\mathrm{erfc}\,(\eta_0/\sqrt{2})}\right.$$
$$\left. +\sigma\left\{1 - \exp\left(\frac{\eta_0^2 - \eta^2}{2}\right)\right\}\right] \tag{4.41}$$

in the preheat zone ($\eta > \eta_0$) and

$$\xi\Theta_\xi^{(1)} - \eta\Theta_\eta^{(1)} - \Theta_{\xi\xi}^{(1)} - \Theta_{\eta\eta}^{(1)} = 0 \tag{4.42}$$

behind the premixed flame. At the premixed flame surface $\eta = \eta_0$, either the fuel or oxidizer mass fraction must vanish, a condition that may be written in the form

$$\Theta(\xi, \eta_0) = \begin{cases} 2(1 - Z(\xi, \eta_0)) & \text{if } \xi \geqslant 0 \\ 2Z(\xi, \eta_0) & \text{if } \xi < 0. \end{cases} \tag{4.43}$$

Substitution of (4.19) and (4.5) then determines the following boundary condition for $\Theta^{(1)}$:

$$\Theta^{(1)}(\xi, \eta_0) = -2a|\zeta(\xi, \eta_0)| = -2a\eta_0|\xi|, \tag{4.44}$$

where a is given by (4.37). The solution to (4.41) and (4.44) in the preheat zone ($\eta > \eta_0$) may be written as

$$\Theta^{(1)}(\xi, \eta) = T_0(\eta) + T_1(\xi, \eta), \tag{4.45}$$

where $T_0(\eta)$ is the solution of the system

$$T_0'' + \eta T_0' = -\sigma\exp\left(\frac{\eta_0^2 - \eta^2}{2}\right)\left[\frac{\eta\,\mathrm{erfc}\,(\eta/\sqrt{2})}{\mathrm{erfc}\,(\eta_0/\sqrt{2})} + \sigma\left\{1 - \exp\left(\frac{\eta_0^2 - \eta^2}{2}\right)\right\}\right] \tag{4.46}$$

and

$$T_0(\eta_0) = T_0(\infty) = 0, \tag{4.47}$$

and $T_1(\xi, \eta)$ is the solution of the homogeneous system

$$\xi\frac{\partial T_1}{\partial \xi} - \eta\frac{\partial T_1}{\partial \eta} - \frac{\partial^2 T_1}{\partial \xi^2} - \frac{\partial^2 T_1}{\partial \eta^2} = 0 \tag{4.48}$$

with boundary condition

$$T_1(\xi, \eta_0) = -2a\eta_0|\xi|. \tag{4.49}$$

The solution for T_1 is readily written down in analogy to (3.16):

$$T_1(\xi, \eta) = \exp\left[(\eta_0^2 - \eta^2)/4\right]\sum_{n=0}^{\infty} b_n H_n(\xi)U(n + 1/2, \eta) \tag{4.50}$$

with b_n defined as follows:

$$b_n = -2a\eta_0 \frac{\displaystyle\int_{-\infty}^{+\infty} |\xi| H_n(\xi) \exp(-\xi^2)\, \mathrm{d}\xi}{2^n n! \sqrt{\pi} U(n+1/2, \eta_0)}. \tag{4.51}$$

We do not need the full solution for $\Theta^{(1)}$ but only need $\Theta_\eta(\xi, \eta_0)$ to generate the matching condition for the inner solution that will determine the flame speed and curvature. From the solution (4.50) it is clear that $\partial_\eta T_1(\xi, \eta_0) \sim \mu \sim O(1/\beta)$ since we are in the regime $B = \mu\beta \sim 1$. Therefore,

$$\Theta_\eta^{(1)}(\xi, \eta_0) = T_0'(\eta_0) + O(1/\beta). \tag{4.52}$$

We now determine $T_0'(\eta_0)$. The general solution to the homogeneous part of (4.46) (that is, the solution to (4.46) if the right-hand side were zero) is

$$T_0(\eta) = -\sqrt{\pi/2}\, A\, \mathrm{erfc}\,(\eta/\sqrt{2}) + B, \tag{4.53}$$

where A and B are arbitrary constants. We now seek to solve (4.46) by using the method of variation of parameters. For this purpose we substitute (4.53) in (4.46) regarding A and B as unknown functions of η. It is readily seen that (4.53) satisfies (4.46) if $A(\eta)$ and $B(\eta)$ are made to satisfy the equations

$$A'(\eta) = -g(\eta), \tag{4.54}$$

$$B'(\eta) = \sqrt{\pi/2}\, \mathrm{erfc}\,(\eta/\sqrt{2}) A(\eta) = -\sqrt{\pi/2}\, \mathrm{erfc}\,(\eta/\sqrt{2}) g(\eta), \tag{4.55}$$

where the function $g(\eta)$ is defined as

$$g(\eta) = \sigma \exp(\eta_0^2/2) \left[\frac{\eta\, \mathrm{erfc}\,(\eta/\sqrt{2})}{\mathrm{erfc}\,(\eta_0/\sqrt{2})} + \sigma \left\{ 1 - \exp\left(\frac{\eta_0^2 - \eta^2}{2} \right) \right\} \right]. \tag{4.56}$$

The boundary conditions (4.47) imply

$$B(\infty) = 0, \tag{4.57}$$

so that (4.55) may be integrated once to give

$$B(\eta_0) = \sqrt{\frac{\pi}{2}} \int_{\eta_0}^{\infty} \mathrm{erfc}\left(\frac{\eta}{\sqrt{2}} \right) g(\eta)\, \mathrm{d}\eta. \tag{4.58}$$

It follows from (4.53) and the boundary condition $T_0(\eta_0) = 0$ that

$$A(\eta_0) = \sqrt{\frac{2}{\pi}} \frac{B(\eta_0)}{\mathrm{erfc}\,(\eta_0/\sqrt{2})}. \tag{4.59}$$

From (4.53)–(4.55) and (4.59),

$$T_0'(\eta_0) = \sigma B(\eta_0). \tag{4.60}$$

If $g(\eta)$ is introduced into (4.58) from (4.56), some of the resulting integrals can be evaluated in closed form so that we get the final result

$$\Theta_\eta^{(1)}(\xi, \eta_0) = T'(\eta_0) + O(1/\beta) = \sigma \mathscr{I}(\eta_0) + O(1/\beta) \tag{4.61}$$

where

$$\mathscr{I}(\eta_0) \equiv \sigma^2 \left[\pi \exp(\eta_0^2) \int_{\eta_0/\sqrt{2}}^{\infty} x\, \mathrm{erfc}^2(x)\, \mathrm{d}x - \frac{\eta_0}{\sigma} + 1 - \frac{1}{2\sigma^2} \right]. \tag{4.62}$$

4.4. *The inner solution and asymptotic matching*

In the case of a small but finite α, the procedure for obtaining the inner solution and carrying out the asymptotic matching is essentially the same as presented in §3.1.2 with the following minor modifications.

(*a*) In the reaction rate term, one must use the modified Z-field as derived in §4.2 so that μ is replaced by μ' which is given by (4.39).

(*b*) A multiplicative factor $(1 - \alpha)^{2\nu}$ appears in the reaction rate term on account of the density dependence of the reaction rate.

(*c*) When matching the temperature gradients at the edge of the reaction zone, we must use the modified outer solution, that is $\Theta_\eta^{(0)}(\xi, \eta_0) + \alpha\Theta_\eta^{(1)}(\xi, \eta_0)$, where $\Theta_\eta^{(1)}(\xi, \eta_0)$ is given by (4.61).

Note that the modification of the advection term in (3.23) due to heat release effects does not affect the inner solution except through the asymptotic matching. This is because, when the equation is written in terms of inner variables, the advection term drops out at leading order.

As a result of this procedure, we get in place of (3.38)–(3.40) the following equations that take into account the effect of heat release at leading order:

$$\frac{U_\infty}{U_\infty^S(\alpha)} = \frac{\eta_0}{\sigma}\left[1 + \alpha\mathscr{I}(\eta_0)\right], \tag{4.63}$$

$$\frac{k}{U_\infty^S(\alpha)}\frac{1}{Z_s}\left(\frac{\partial Z}{\partial y}\right)_0 = \frac{\sqrt{4\nu - 2}}{\beta}\frac{1}{\eta_0^2}\frac{U_\infty}{U_\infty^S(\alpha)}, \tag{4.64}$$

$$\frac{k}{U_\infty^S(\alpha)}\kappa = \frac{1}{\eta_0^2}\frac{U_\infty}{U_\infty^S(\alpha)}, \tag{4.65}$$

where the flame speed is now normalized by the speed of the stoichiometric planar flame with small but finite α,

$$U_\infty^S(\alpha) = (1 - \alpha)^\nu U_\infty^S, \tag{4.66}$$

U_∞^S being the corresponding speed without heat release effects as given by (3.37). In (4.63), (4.64), and (4.65) σ and $\mathscr{I}(\eta_0)$ are expressions involving η_0 as defined in (4.8) and (4.62) respectively. The suffix in the mixture fraction gradient term, $(\partial Z/\partial y)_0$, indicates that this quantity is evaluated at the tip of the triple flame. This is related to the value of the mixture fraction gradient $(\partial Z/\partial y)_\infty$ far upstream through (4.39), which may be written in terms of dimensional variables as

$$\left(\frac{\partial Z}{\partial y}\right)_0 = \left(\frac{\partial Z}{\partial y}\right)_\infty\left[1 + \frac{\alpha}{2}(1 + \sigma\eta_0 - \eta_0^2)\right]^{-1}, \tag{4.67}$$

where we have used the result $(1 - \alpha A)^{-1} = 1 + \alpha A + O(\alpha^2)$ (where A is any quantity independent of α) to put these equations in a form that does not admit unphysical values even if α is not necessarily small, though the results may not be reliable unless $\alpha \ll 1$.

In the special case where both the curvature κ and α are small one could perform an asymptotic expansion in (4.63)–(4.67) with respect to the large parameter η_0 and obtain as a result the following limiting form valid in the limit $\alpha \ll 1$ and $\kappa \ll 1$:

$$\frac{U_\infty}{U_\infty^S(\alpha)} = 1 + \alpha - \frac{k}{U_\infty^S(\alpha)}\kappa, \tag{4.68}$$

$$\kappa = \frac{\beta}{\sqrt{4v-2}} \frac{1}{Z_s} \left(\frac{\partial Z}{\partial y}\right)_0, \tag{4.69}$$

$$\left(\frac{\partial Z}{\partial y}\right)_0 = \frac{1}{1+\alpha} \left(\frac{\partial Z}{\partial y}\right)_\infty. \tag{4.70}$$

4.5. *Discussion of the solution*

Heat release has two distinct qualitative effects on the propagation speed of the triple flame. First, the reduction in the fluid velocity in front of the flame due to the effect of heat release results in an increased propagation speed through the mechanism of streamline divergence. This effect appears in (4.63) as the additive term proportional to α in the numerator. Secondly, the mixture fraction gradient in front of the triple flame is reduced by the streamline divergence. This results in a reduced curvature, thereby a reduced heat loss and consequently an increased propagation speed. This effect is taken into account by the terms in the square brackets on the right-hand side of (4.67).

The effect of heat release on the propagation speed is shown in figure 11, where the triple-flame speed (normalized by the planar flame speed) is plotted against the dimensionless mixture fraction gradient (abbreviated as MFG in the figures) which is defined as $(k/U_\infty^S(\alpha))Z_s^{-1}(\partial Z/\partial y)$ evaluated at the flame tip. The symbols are obtained from an earlier numerical simulation of the full compressible equations by Ruetsch *et al.* (1995) and the solid line is the present theoretical result given by equations (4.63) and (4.64). Also shown (dashed line), is the result that would be obtained if the effects of heat release were neglected in the theory ($\alpha = 0$). It is clear that for $\alpha = 0.75$ the correction due to heat release is significant. The deviation from the simulation data is of the order of 10%, which is rather remarkable taking into account the fact that $\alpha = 0.75$ cannot be considered a very small parameter! This gives reason to hope that, even though the theory has been developed for small heat release, the results can be used with some confidence in the more realistic parameter regime, $\alpha \sim 0.8$. The numerical simulations of Ruetsch *et al.* (1995) used temperature-dependent transport coefficients but the transport coefficients are assumed constant in our theory. Some of the simulations of Ruetsch *et al.* (1995) were therefore repeated with constant values of transport coefficients but this did not change the normalized flame propagation speed in any noticeable way. The theoretical prediction, (4.67), for the reduction of the mixture fraction gradient due to flow divergence however could not be checked against the simulation data. This is because, in the simulations, a tan-hyperbolic profile is assumed for the Z-field instead of the simpler linear profile used in the present theory. As a result, the mixture fraction gradient decreases downstream simply due to diffusive spreading while the strictly linear profile will show no such effect. Thus, 'upstream mixture fraction gradient' is ambiguous for this freely expanding mixing layer. An acceptable substitute might be the mixture fraction gradient at the triple-flame location for an otherwise identical simulation but without the flame. Unfortunately, these data are not available in the paper by Ruetsch *et al.* (1995). In the simulation data, the ratio of the mixture fraction gradient, at the flame tip to its value at the inlet of the computational box decreases rapidly with increasing mixture fraction gradient, showing that any effect of the flow divergence is masked by the diffusive spreading of the mixing layer. According to the theory, this ratio should increase slowly with increasing mixture fraction gradient for a strictly linear mixture fraction profile.
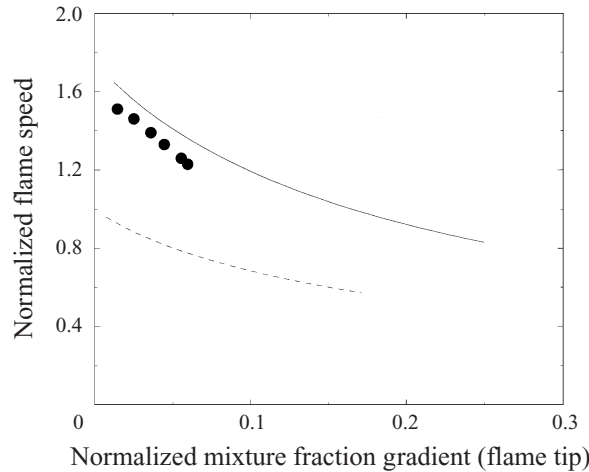
FIGURE 11. The normalized speed of the triple flame as a function of the dimensionless MFG at the flame tip for $\alpha = 0.75$ and $\beta = 8$ as obtained from numerical simulations by Ruetsch *et al.* (1995) (symbols), theory with heat release effects included (solid line), theory without heat release effects (dashed line).

A second set of four numerical simulations was performed using the same methodology as described in Ruetsch *et al.* (1995) but for a lower value of the heat release parameter, $\alpha = 0.3$, and varying mixture fraction gradients. For better correspondence with the theory we chose constant transport coefficients in these runs. The simulations were re-run with identical values of all parameters but this time without the triple flame. The values of the mixture fraction gradient were computed at the locations where the flame tip of the triple flame would have been. Then this value can reasonably be identified with the 'upstream mixture fraction gradient' used in the theory where the Z-profile is strictly linear so that this quantity can be defined without ambiguity. The ratio of the mixture fraction gradient at the triple point to the corresponding value when there is no flame is plotted in figure 12. The symbols are the results of the numerical simulations while the solid line represents the theory given by equations (4.63)–(4.67). In the case of a real flame, which has a finite thickness, the definition of 'the flame tip' is somewhat ambiguous. In figure 12, the square symbols correspond to the situation where the flame tip is identified as the point where the X-component of the fluid velocity is a minimum while the round symbols correspond to the situation where the flame tip is identified as the point where the reaction rate is a maximum. Both determinations are shown in figure 12 so as to give some indication of the degree of uncertainty inherent in the simulation data. Figure 13 shows the normalized triple-flame speed as a function of the normalized mixture fraction gradient at the triple point for the simulations with $\alpha = 0.3$. The agreement between theory and simulation is seen to be better than for $\alpha = 0.75$ shown in figure 11. This is what one would expect from a theory valid at small α.

Figure 14(a) shows the X-component of the fluid velocity along the X-axis normalized by the flow speed far upstream (which is the triple-flame propagation speed). The independent variable is $X = xU_{\infty}^{S}(\alpha)/k$, where x is in physical units. The simulation corresponds to a dimensionless mixture fraction gradient of 0.063 at the flame tip. The results for the simulation runs with the other three mixture fraction values are very similar and are therefore not shown. The dashed line is the result of the numerical simulation and the solid line is the asymptotic result (4.17). Where the normalized
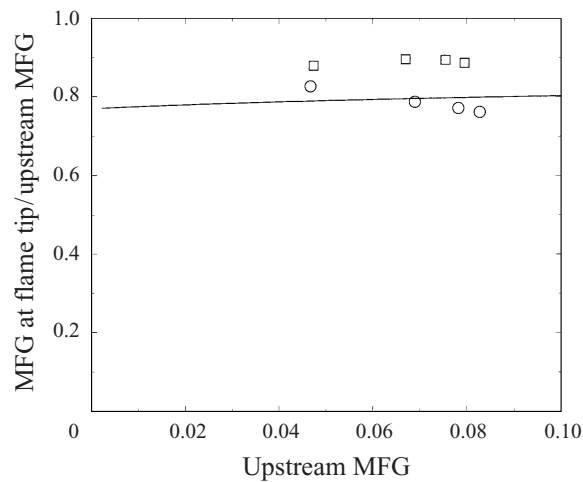
FIGURE 12. The ratio of the MFG at the flame tip to the MFG at the same location in the absence of the flame for a fixed $\alpha = 0.3$ and $\beta = 8$ as obtained from numerical simulations (symbols) and theory (solid line). The two types of symbols correspond to two different ways of defining the flame tip (see text).
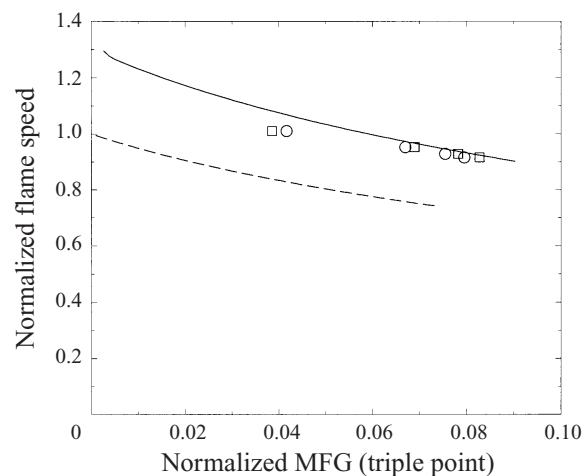

FIGURE 13. The normalized speed of the triple flame as a function of the dimensionless MFG at the flame tip for $\alpha = 0.3$ and $\beta = 8$ as obtained from numerical simulations (symbols), theory with heat release effects included (solid line), theory without heat release effects (dashed line). The two types of symbols correspond to two different ways of defining the flame tip (see text).

triple-flame speed is required to generate the curves, we use the theoretical value for the theoretical curve and the simulation result for the curve showing simulation data. It is seen that in the preheat zone, the two curves do have the same qualitative shape. However, the theoretical curve does not asymptote to unity far upstream quite as fast as the simulation data. Further, the theory overpredicts the dip in fluid velocity in front of the flame, and, unlike the simulation data, does not overshoot the upstream fluid speed upon crossing the flame front. Figure 14(*b*) compares the Y-component of the velocity along the Y-axis given by the asymptotic result (4.18) (solid line) with the corresponding numerical simulation data (dashed line). The agreement of the two results is excellent. The excellent prediction of the Y-component of the velocity is
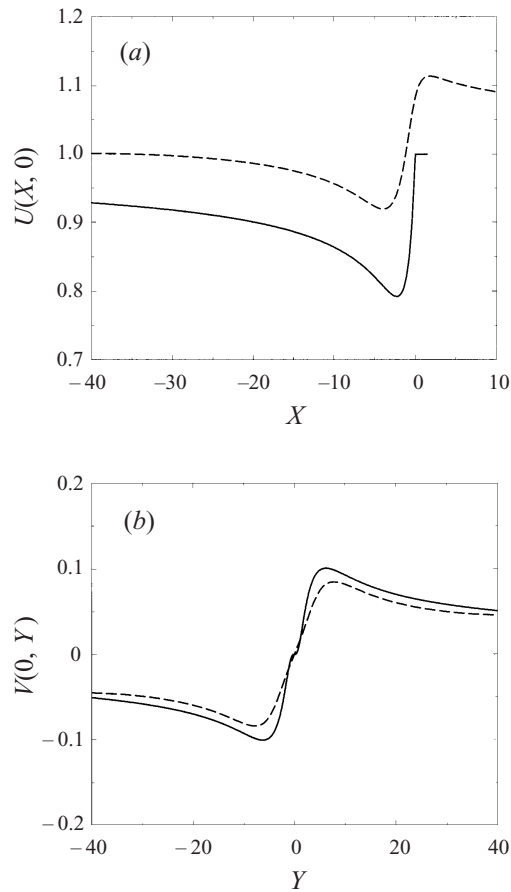
FIGURE 14. (*a*) The X-component and (*b*) the Y-component of the fluid velocity (normalized by the triple-flame speed) along the X-axis and Y-axis respectively according to theory (solid line) and according to numerical simulations (dashed line).

quite fortunate, because this is the critical component that enters into the theoretical prediction for the triple-flame speed. The perturbation of the X-component of the velocity does not enter into the theoretical prediction for the flame speed, since its effect is felt at a higher order.

5. Conclusions

An approximate theory was presented for triple flames in the limit of large activation energy (large β) and small but finite heat release (α small but non-zero) using the parabolic flame path approximation. Explicit analytical formulas were presented for determining the flame propagation speed and the curvature of the triple flame. The temperature, velocity and reaction rates were expressed analytically. The triple flame is in fact completely characterized through explicit analytical representation once a single parameter – the upstream mixture fraction gradient – is known. Detailed comparisons were made between the theory and numerical simulations of the primitive equations. Generally good agreement between theory and numerics was observed and the discrepancies between the two were generally within expected bounds.

The most important simplification that permitted us to obtain these analytical results was the replacement of the curved flame front by a parabolic profile, thereby reducing a free boundary problem to one in which the boundary is known except for a single parameter, the curvature of the parabola.

Using particle image velocimetry, Muñiz & Mungal (1997) have measured instantaneous two-dimensional velocity fields at the location where combustion starts in a lifted jet flame. Their results show that the zone where the flame is stabilized moves within the turbulent flow, following the location of the low-velocity region of the jet. The fluid velocity at the stabilization point was found to take values close to the stoichiometric premixed laminar flame speed. Moreover, the velocity profiles measured across the flame base features properties similar to those observed in numerical simulations of triple flames. One may then believe that, in addition to the fundamental insight and satisfaction that an analytical solution provides, the results presented in this paper could serve as a starting point for a simplified description of more complex problems of technological importance, and to provide important insight for physical understanding of numerical or experimental observations.

REFERENCES

ABRAMOWITZ, M. & STEGUN, I. A. 1970 *Handbook of Mathematical Functions*. Dover.

BRAY, K. N. C. 1996 The challenge of turbulent combustion. In *Proc. 26th Symp. (Intl) on Combustion, Naples* The Combustion Institute, Pittsburgh.

BUCKMASTER, J. & MATALON, M. 1988 Anomalous Lewis number effects in tribrachial flames. In *Proc. 22nd Symp. (Intl) on Combustion*, pp. 1527–1535. The Combustion Institute, Pittsburgh.

BUCKMASTER, J. & WEBER, R. 1996 Edge-flame holding. In *Proc. 26th Symp. (Intl) on Combustion*. The Combustion Institute, Pittsburgh.

BURKE, S. P. & SCHUMANN, T. E. W. 1928 Diffusion flames. *Indust. Engng Chem.* **20**, 998–1004.

CHOI, H. J., KO, Y. S. & CHUNG, S. H. 1998 Flame propagation along a nonpremixed vortex ring. *Combust. Sci. Tech.* **139**, 277–292.

COHEN-TANNOUDJI, C., DIEU, B. & LALOE, F. 1977 *Quantum Mechanics*, Vol. I. John Wiley.

DAOU, J. & LIÑÁN, A. 1998 The role of unequal diffusivities in ignition and extinction fronts in strained mixing layers. *Combust. Theory & Modelling* **2**, 449–477.

DOLD, J. W. 1994 Triple flame as agent for restructuring of diffusion flame. In *Proc. Zel'Dovich Memorial, Institute of Structural Macrokinetics, Chernogolovka, Russia* (ed. A. G. Mershanov & S. M. Frolov), pp. 7–19.

DOLD, J. W. 1989 Flame propagation in a nonuniform mixture: analysis of a slowly varying triple flame. *Combust. Flame* **76**, 71–88.

DOMINGO, P. & VERVISCH, L. 1996 Triple flames and partially premixed combustion in autoignition of nonpremixed mixtures In *Proc. 26th Symp. (Intl) on Combustion, Naples*, pp. 233–240. The Combustion Institute, Pittsburgh.

ECHEKKI, T. & CHEN, J. H. 1998 Structure and propagation of methanol-air triple flames. *Combust. Flame* **114**, 231–245.

FAVIER, V. & VERVISCH, L. 1998 Investigating the effects of edge-flames in liftoff in non-premixed turbulent combustion. In *Proc. 27th Symp. (Intl) on Combustion, Boulder, CO*. The Combustion Institute, Pittsburgh.

HARTLEY, L. J. & DOLD, J. W. 1991 Flame propagation in a nonuniform mixture: analysis of a propagating triple-flame. *Combust. Sci. Tech.* **80**, 23–46.

KIONI, P. N., ROGG, B., BRAY, K. N. C. & LIÑÁN, A. 1993 Flame spread in laminar mixing layers: the triple flame. *Combust. Flame* **95**, 276–290.

LELE, S. K. 1992 Compact finite difference schemes with spectral-like resolution. *J. Comput. Phys.* **103**, 16–42.

LIÑÁN, A. & CRESPO, A. 1976 An asymptotic analysis of unsteady diffusion flames for large activation energies. *Combust. Sci. Tech.* **14**, 95–117.

LIÑÁN, A. & WILLIAMS, F. A. 1993 *Fundamental Aspects of Combustion*. Oxford University Press.

MUÑIZ, L. & MUNGAL, M. G. 1997 Instantaneous flame-stabilization velocities in lifted-Jet diffusion flames. *Combust. Flame* **111**, 16–31.

PETERS, N. 1982 Discussion of test problem A. In *Numerical Methods in Laminar Flame Propagation, GAMM-Workshop* (ed. N. Peters & J. Warnatz), pp. 1–14. Vieweg & Sohn.

PHILLIPS, H. 1965 Flame in a buoyant methane layer. In *Proc. 10th Symp. (Intl) on Combustion*, pp. 1277–1287. The Combustion Institute, Pittsburgh.

PLESSING, T., TERHOEVEN, P., PETERS, N. & MANSOUR, M. S. 1998 An experimental and numerical study of a laminar triple flame. *Combust. Flame* **115**, 335–353.

POINSOT, T. & LELE, S. K. 1992 Boundary conditions for direct simulations of compressible viscous flows. *J. Comput. Phys.* **101**, 104–129.

RUETSCH, G., VERVISCH, L. & LIÑÁN, A. 1995 Effects of heat release on triple flames. *Phys. Fluids* **6**, 1447–1454.

VAN DYKE, M. 1975 *Perturbation Methods in Fluid Mechanics*. The Parabolic Press.

VERVISCH, L. & POINSOT, T. 1998 Direct numerical simulation of non-premixed turbulent flames. *Ann. Rev. Fluid Mech.* **30**, 655–692.

WILLIAMS, F. A. 1985 *Combustion Theory*. Benjamin/Cummings.